atmosphere

MDPI

Article

Seasonal and Botanical Influences on External Thermal Performance near Green Façades: CFD Simulations on a Reference Building Envelope in a Humid Temperate Climate

Barbara Gherri [1,*], Lisa Rovetta [1], Sara Matoti [1,2] and Alessandro Petraglia [3]

[1] Department of Engineering and Architecture, Università di Parma, 43124 Parma, Italy; lisa.rovetta@unipr.it (L.R.); sara.matoti@unipr.it (S.M.)
[2] Department of Classics, Sapienza Università di Roma (IT), 00185 Roma, Italy
[3] Department of Chemistry, Life Sciences and Environmental Sustainability, Università di Parma, 43124 Parma, Italy; alessandro.petraglia@unipr.it
* Correspondence: barbara.gherri@unipr.it; Tel.: +39-0521905956

Abstract

Green façades are acknowledged as passive strategies that reduce heat accumulation, enhance biodiversity, improve particulate matter absorption and provide psycho-physiological benefits for users. However, evaluations of their thermal performance—accounting for seasonality, vegetation density, and leaf characteristics—remain incomplete. This study addresses this gap by assessing two green façade typologies on a sample building located in Northern Italy (Cfa climate). ENVI-met microclimate simulations compared a bare wall with vegetated façades featuring *Hedera helix* (evergreen) and *Parthenocissus tricuspidata* (deciduous) across four orientations and seasonal conditions, considering the sample building and the immediate surrounding outdoor space. Both species reduced wall-surface temperatures (T_0) and improved outdoor thermal comfort perception (PET), influenced by LAI dynamics, foliage persistence, and façade orientation. Results indicate that *Parthenocissus tricuspidata* achieved the greatest cooling effect during hot periods due to higher LAI, with absolute T_0 reductions of up to 22.1 °C on southern façades and 30.0 °C on western façades. In these orientations, PET improvements reached up to 3.0 °C (south) and 8.0 °C (west). Conversely, *Hedera helix* ensured stable year-round performance and performed better on northern façades during colder periods. The results stress the need for integrated design that aligns plant choice with orientation and seasonal growth to optimize thermal performance, cut cooling demands, and improve outdoor comfort.

Keywords: green façades; microclimatic assessment; leaf area index; façade orientation; *Parthenocissus tricuspidata*; *Hedera helix*

Check for updates

Academic Editors: Gianni Bellocchi, Stefano Cascone, Vincenzo Di Naso, Frida Bazzocchi and Cecilia Ciacci

Received: 28 January 2026
Revised: 24 March 2026
Accepted: 25 March 2026
Published: 28 March 2026

Copyright: © 2026 by the authors. Licensee MDPI, Basel, Switzerland. This article is an open access article distributed under the terms and conditions of the Creative Commons Attribution (CC BY) license.

1. Introduction

Green roofs and green walls are increasingly being implemented in urban areas, contributing a novel dimension to urban green infrastructure [1]. The potential of green building roofs and façades can be more actively harnessed to achieve diverse environmental benefits.

Research and practical application have predominantly focused on green roofs [2,3], rather than green walls [4]. Moreover, the specific literature on green façades is quite limited. To advance the adoption of green walls, the existing knowledge should be expanded through targeted research that informs architectural design, botanical knowledge and building management [5].

In recent years, a considerable body of literature has emerged on green walls, primarily addressing their thermal and energy-related properties, in addition to studies that consider how urban vegetation can affect air quality by influencing pollutant deposition and dispersion [6,7]. Experimental investigations have assessed reductions in the heat flux into indoor environments, thereby decreasing cooling demands. Overall, the thermal efficacy of green walls varies depending on design and constituent elements, such as plant species, the presence and composition of any type of substrate, the presence and type of container, irrigation methods, and the thermal insulation properties of the building envelope.

From a building technological perspective, green walls, also referred to as Vertical Greening Systems (VGSs) [8–10], indicate solutions intended to facilitate the cultivation of vegetation on vertical building surfaces, exploiting various plant species. Technologically, green walls are classified into two primary types [11]: green façades (GFs) and living walls (LWs) [12,13]. Green façades [14] typically involve climbing plants that grow directly on walls through their aerial roots, leaf tendrils, lianas, vines, and scramblers. Therefore, GFs are characterized by minimal technological components. Most green façades do not require irrigation, and their maintenance needs are the lowest compared to other green solutions. In contrast, living walls, which can be either modular or continuous, promote more uniform vegetation growth across their surface and support a greater diversity of plant species. However, LW systems require regular irrigation and nutrient supplementation.

GFs offer a wide variety of benefits, including low maintenance requirements: a limited level of integration between plants and walls can be seen, since these systems primarily rely on the botanical characteristics of climbing species to grow directly by attaching their roots or aerial roots to the vertical surfaces of backside walls [15]. Therefore, GFs are lightweight, easy to install, and generally require low maintenance.

In urban environments, green walls are primarily valued for their aesthetic properties and thermal benefits.

The most-acknowledged results demonstrate that, during hot summer days, green walls can lower the temperature of the wall surface by approximately 6.0–7.0 °C [16], ensuring an up to 40% temperature reduction in comparison to a plastered wall [17]. Research suggests that green walls can retain heat accumulated during the day, thereby mitigating the extent of indoor cooling required at night, in addition to lowering ambient urban air temperatures by over 1.0 °C [18].

Generally, four primary mechanisms define green systems as passive strategies for energy conservation: (i) the interception of solar radiation resulting from the shading effect of vegetation [19]; (ii) the thermal insulation afforded by both the vegetation and the substrate [20]; the evaporative cooling facilitated by evapotranspiration from the plants and substrate [21–23]; and, lastly, the modulation of wind effects on the building [24].

More specifically, the significant potential of vegetation applied to building façades to reduce energy demands varies according to climate, building type, and envelope and vegetation type. Previous studies within a Mediterranean continental climate [25] have demonstrated that vertical greening system can passively decrease a building's energy consumption by up to 34% during the cooling season (in the case of a double-skin green façade) and up to 59% for a green wall.

Precise studies conducted in hot climates [26,27] found that having leaf cover on buildings facing the equator consistently cools indoor temperatures by about 5.0 °C during summer. This effect reduced indoor temperature range from 17.0–33.0 °C to 18.0–28.0 °C when outdoor temperatures ranged from 21.0 °C to 31.0 °C. In winter, leaf cover also decreased indoor temperature fluctuations, narrowing the range from 10.0–30.0 °C without leaf coverage to 12.0–27.0 °C in the case of the vegetation treatment, while outdoor temperatures ranged from

7.0 °C to 18.0 °C. Overall, leaf cover helps moderate indoor temperatures year-round when applied in hot climates.

Over time, several studies have investigated green walls and façades' cost savings and other economic benefits. Specific studies have also been conducted on life cycle assessments of green façades [28]. Since green façades usually have slow surface coverage and include a limited plant selection, incomplete data are available in terms of energy savings and cost benefit.

Expanding considerations from the building to the urban sphere (although the urban realm is not the focus of the present research), a broad body of research has evaluated living walls and green façades as effective methods to mitigate the urban heat island effect [1,29,30]. The results generally prove that, regardless of geographical location, green walls reduce temperature fluctuations [31] by decreasing the maximum temperature and increasing the minimum temperature [32,33]. The relevance of green façades becomes particularly evident in high-density urban contexts, where compact morphologies, a reduced sky-view factor, and deep street canyons intensify heat accumulation and limit natural ventilation, as demonstrated in He et al. (2021) [34] and in Carlo et al. (2024) [35]. Similar findings [36,37] confirm that dense built environments experience stronger microclimatic stress due to continuous hard surfaces and restricted airflow. In this framework, green façades represent an effective and space-efficient intervention capable of providing shading, improving evapotranspiration, and enhancing thermal comfort precisely where conventional horizontal greening is most constrained.

Eventually, a limited body of research has examined the impact of green walls on adjacent air temperature and Mean Radiant Temperature, MRT [38], as well as on thermal perceptions [39]. These studies have primarily relied on quantitative simulations, with few experimental setups conducted.

1.1. LAI for Green Façade Performance

According to the existing literature, the most common climbers used in the case of both spontaneous and man-made green façades are *Hedera helix* (English ivy), *Parthenocissus tricuspidata* (Boston ivy), *Parthenocissus quinquefolia* (Virginia creeper) and *Vitis vinifera* (grape), whose coverage can cover a depth of up to 200 mm.

However, the current literature remains incomplete because most studies rely on short-term or single-season analyses, which fail to capture full annual LAI variability—especially for deciduous species whose foliage changes substantially. Research also reports inconsistent LAI values and rarely integrates LAI with other key factors such as foliage thickness, phenology, façade orientation, or building-envelope properties. Furthermore, winter and transitional-season performance remain understudied, leaving the combined effects of radiative, convective, and seasonal dynamics insufficiently understood.

The thermal performance of a green façade depends on multiple factors, including plant-related characteristics—such as percentage of coverage, foliage density, and foliage width—as well as building-envelope attributes, including façade orientation, the presence and position of thermal insulation within the masonry, and the solar absorption coefficient of the façade. Local climatic conditions also play a significant role. Among the parameters influencing the thermal benefits of green façades, the leaf area index (LAI), defined as the ratio of leaf cross-sectional area to the unit area covered, is particularly relevant. LAI represents a critical plant attribute, as the primary mechanisms underlying plant-mediated cooling are solar shading and latent heat loss through evapotranspiration. However, previous research has rarely investigated or compared the influence of LAI on the thermal performance of green façades, despite its recognized importance [40]. Recently, LAI has been widely used to compare plant species applied in green façades [41], to monitor plant

growth and maturity, and to evaluate seasonal variations in energy-saving performance. Nevertheless, its influence on thermal performance remains insufficiently supported by multidisciplinary and transdisciplinary research. This limitation is largely due to the high variability of LAI values reported in the literature, often derived from a limited range of plant species and based on average values that do not capture seasonal variations, particularly in deciduous species.

Moreover, most studies have focused primarily on cooling periods, underestimating the impact of green façades on thermal performance during the heating season. LAI has been shown to significantly influence cooling efficacy, with several studies reporting reductions in exterior wall-surface temperatures, although results vary widely. Reported temperature decreases range from 1.0 °C to 31.9 °C, including a 15.8 °C summer reduction in Lleida, Spain, due to *Wisteria sinensis* coverage [42], and a 5.7 °C decrease on an eastern wall covered by *Parthenocissus tricuspidata* in Greece [32]. Detailed studies [43] have also indicated that summer energy savings from green façades are strongly influenced by building orientation [44].

A major limitation in the literature is the lack of integration between LAI values, botanical species selection, seasonal assessment, and wall orientation. In addition, most studies rely on on-site measurements, which limits comparability across investigations. Another limitation concerns the continuous annual variation in LAI, particularly for evergreen climbers. While continuous LAI measurement is standard in agricultural research—typically performed on horizontal planes—its application to vertical green façades, considering wall orientation and inter-species comparison, remains largely unexplored.

1.2. Leaf Temperatures and Foliage Thickness

Additional parameters exerting a great influence on green façade thermal behavior are leaf temperatures and foliage thickness.

Leaf temperature is a complex parameter to determine. Several studies were conducted in the past [45] by measuring temperature via infrared radiometer and other thermometers [46]. Research has demonstrated that sunlit leaves can be approximately 20.0 °C warmer than the surrounding air temperature, while shaded leaves can register temperatures about 1.5 °C below the air temperature during daytime [47].

The complexity of foliage temperature evaluation arises from the sophisticated energy exchanges involved in the leaf, including energy absorption, convective heat exchange, and transpiration. Due to this complexity, a few studies—mostly empirical—have shown that transpiration plays a relatively strong role in reducing leaf temperatures, whereas convection is a relatively inefficient cooling process.

Most of the studies on the effect of foliage thickness on thermal performance of green façades are performed via field measurements [48]: quite obviously, wall-surface temperature results showed clear variability between a bare wall and a covered wall, with a maximum temperature reduction around noon, attesting to the benefits of dense foliage coverage during daytime. At nighttime, the wall temperature difference between the covered wall and the bare wall was relatively small. When measuring the temperature under leaf surfaces, it was usually higher than the exterior wall's surface temperatures, especially in the daytime, but the opposite trend was observed in the evening and nighttime.

Based on field measurements in a hot and humid climate, the air near a denser and thicker layer of foliage had a much higher air temperature than the air near thinner layers of leaves, when measured during daytime at 5 cm from the green façade. This demonstrates that with a foliage thickness of about 30 cm, the air temperature above the coverage is higher than it is above thinner layers of leaves due to the dense vegetation, which may block air circulation and raise the air temperature. Once again, most studies cannot

provide a comprehensive annual overview of thermal behavior due to the complexity of measurements. Additional limitations may arise from evaluations conducted on only a limited number of orientations.

1.3. Botanical Species Evaluation for Wall Climbers

For species evaluated under different climatic conditions and wall orientations—such as *Hedera helix*, *Parthenocissus tricuspidata*, *Vitis*, *Jasminum*, *Pyracantha*, *Wisteria sinensis*, *Parthenocissus quinquefolia*, *Ficus pumila*, *Bauhinia corymbosa*, and *Pyrostegia venusta*—thermal performance has been assessed across diverse environmental contexts. These species generally improve building thermal performance by intercepting solar radiation and providing shading effects comparable to architectural elements such as overhangs, slats, and awnings.

Figure 1 illustrates the temperature reduction achieved by façades covered with *Parthenocissus tricuspidata* and *Hedera helix*. The results indicate that *Parthenocissus tricuspidata* performs best during summer, with an average surface temperature decrease of approximately 8.6 °C, while *Hedera helix* achieves a reduction of 7.1 °C in summer and 1.5 °C in autumn.

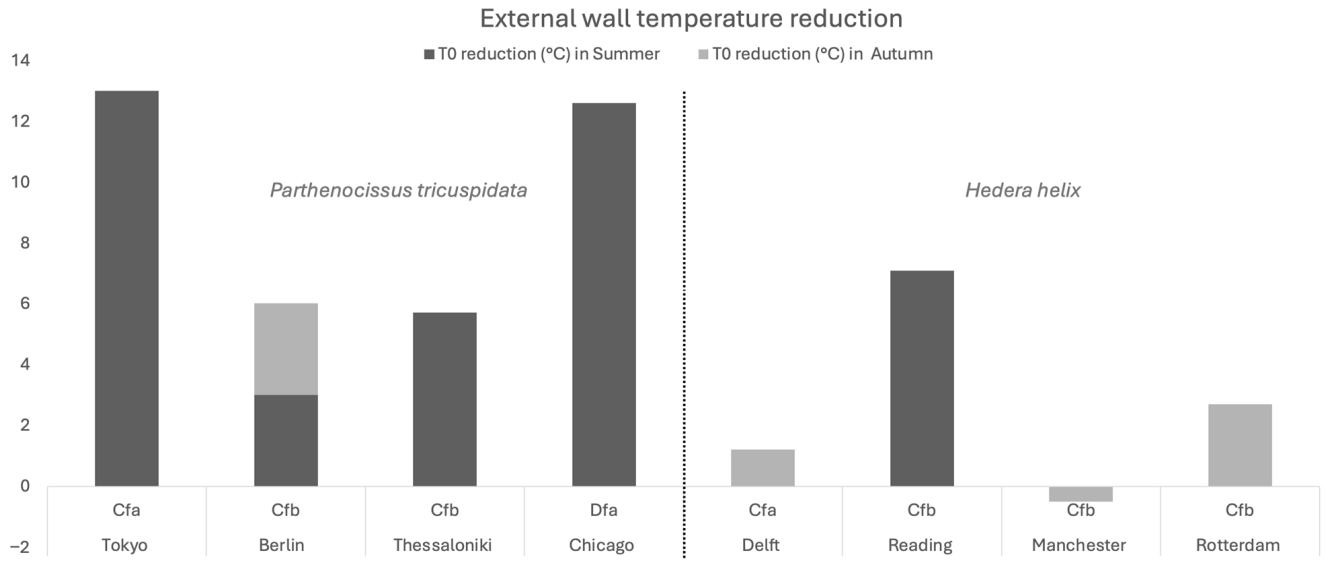


Figure 1. Temperature reduction due to external wall in case of *Parthenocissus tricuspidata* and *Hedera helix* coverage, according to literature.

Among these species, *Hedera helix* has been the subject of the most comprehensive studies. Its popularity is attributed to its evergreen nature, year-round growth, adaptability to climate variability, and high resistance to frost—characteristics that support its widespread distribution across Europe. Botanical research [49] suggests that its propagation has been further facilitated by milder winters associated with climate change.

Recent findings in a temperate climate [50] on *Hedera helix* masonry wall coverage indicate that its application as a green covering can substantially influence the thermal behavior of masonry walls by ensuring an up to 30% lower heat transfer through covered walls compared to uncovered walls (considering winter season). This suggests that *Hedera helix* coverage has the potential to decrease heating energy demand by maintaining a higher temperature beneath the foliage compared to exposed walls during winter, thereby helping to limit moisture accumulation and the associated risk of mold development. Conversely, in the summer months, the surface temperature beneath the ivy was lower than that of the bare wall during the daytime, indicating a possible reduction in cooling energy requirements.

Limited research has been conducted on the thermal benefits of *Parthenocissus tricuspidata*, primarily because it is a deciduous climber with limited practical applications.

In Central Europe, *Hedera helix*, *Parthenocissus tricuspidata*, and *Parthenocissus quinquefolia* are quite common due to the spontaneous proliferation of these climbing plants (although the latter two species are both non-native to Europe).

Parthenocissus tricuspidata is especially prevalent because of its aesthetic appeal, the variation in its foliage color throughout the annual cycle, its thermal regulation properties, its acoustic insulation capabilities, and its ability to reduce particle matter [51]. Moreover, its cooling and energy-saving effects improve as solar radiation intensity and temperature increase [52].

2. Aim and Scope

The body of research on green façades has progressively evolved over the past 20 years, developing into a transdisciplinary field that primarily addresses four key issues: (i) urban greening and sustainability; (ii) thermal behavior, including warming and cooling potential, and energy-saving mechanisms; (iii) on-site measurements of actual thermal and microclimatic performance; and (iv) modeling and simulation approaches.

The relationship between the botanical behavior of climbing species—their growth patterns, foliage density, and coverage—and the four different wall orientations has not been thoroughly investigated. Moreover, most existing studies rely on short-term field measurements.

To address these scientific gaps, this study employs numerical simulations to evaluate the thermal performance of two climbing plant species applied to four wall orientations, considering seasonal variations in leaf area index, LAI. The research adopts a microclimatic modeling approach that integrates technological and botanical parameters to optimize the benefits of green façades in humid temperate climates. Therefore, the focus of this study remains on the building envelope and its thermal exchange with the outdoor environment when covered by different climbing species and across multiple façade orientations.

Specifically, this study investigates the thermal benefits of an evergreen climber compared to those of a deciduous climber across four representative periods, each corresponding to distinct seasonal variations in LAI (namely February, May, July, and October), on a sample building in Northern Italy. The main objective is to evaluate the effects of two green façade systems, applied on all four sides of the building envelope, using two climbing species: *Hedera helix* (evergreen) and *Parthenocissus tricuspidata* (deciduous). The analysis focuses on their impact both on wall-surface temperatures and on the immediate surrounding outdoor environment. This study will consider the two climbers' growing cycles, leaf density, and foliage coverage.

Specifically, this study aims to:

1. Quantify the outdoor surface-wall temperature (T_0) reduction (absolute difference in °C) provided by the two selected species at different phenological stages across four wall orientations, compared to a bare wall.
2. Identify which plant species and foliage density are most effective in reducing wall-surface temperature (T_0) across four orientations during the four selected periods.
3. Analyze the wall temperature profile after sunset during summer to determine whether green façades retain heat or facilitate heat dissipation.
4. Assess the impact of longwave radiation in relation to variations in foliage density.
5. Evaluate how plant type and wall orientation influence outdoor thermal perception, using Physiological Equivalent Temperature, PET, as an indicator.

3. Methodology

The paper investigates the interactions of green façades applied directly to a sample building at two scales: (i) the wall scale, by analyzing temperature variations during key growth stages of the selected species, and (ii) the user scale, by evaluating the potential of green façades to mitigate outdoor thermal stress in the vicinity of the green façades.

A sample building was used to evaluate differences in thermal performance at the building-envelope scale, with a specific focus on the wall-adjacent microclimate rather than on broader, generalized urban-cooling effects. The approach allows for a more precise understanding of how different types of façade greening influence near-surface thermal behavior throughout the year.

The case study building is in Parma (44°48′05.3″ N; 10°19′40.8″ E), Northern Italy, which is classified as a humid subtropical climate (Cfa) according to the Köppen–Geiger system. Despite its classification as humid subtropical (Cfa), climatic trends in Northern Italy, including increasing summer temperatures and more frequent drought-like conditions, suggest a shift toward Mediterranean-like climate characteristics in terms of thermal and precipitation patterns. Observational climate studies show strong warming trends and an intensification of extreme heat events that are consistent with Mediterranean climatic influences in this transition area [53].

The analysis focuses on the year 2024, identified as the hottest year on record based on NASA climate data. During this period, global mean temperatures exceeded the 20th-century baseline (1951–1980) by 1.3 °C, highlighting the relevance of investigating façade greening strategies under extreme thermal conditions.

NASA's Prediction of Worldwide Energy Resources (NASA POWER) dataset [54] provides meteorological variables widely used in energy modeling. In this study, it was preferred over the EPW file due to the need for high-accuracy satellite-derived data and to address data scarcity for the selected location. The EPW file available for Parma is based on heterogeneous historical years—many from the 1970s and 1980s—and therefore fails to capture recent warming trends, overheating episodes, and extreme heat waves recorded in the last decade. Conversely, NASA POWER offers up-to-date satellite-based information that more accurately reflects current climatic conditions, ensuring a more reliable representation of recent thermal patterns for simulations.

NASA POWER provides data at a $0.5^\circ \times 0.5^\circ$ spatial resolution, including daily measurements of near-surface air temperature, relative humidity, precipitation, solar radiation, and wind speed. These variables derive from numerical weather prediction models that integrate multiple observational sources.

The EPW files, by contrast, typically include measured or validated datasets—such as Typical Meteorological Year (TMY) records—constructed from 20 to 30 years of weather-station observations. Although historically consistent, they do not fully represent recent climate-change-driven anomalies [55]. NASA POWER's satellite-based reanalysis offers broader spatial coverage and improved capacity to reflect climate-related trends, despite some limitations. Recent evaluations [56,57] show good performance for maximum and minimum temperatures and solar radiation, while wind speed and relative humidity still require refinement.

Figure 2 illustrates the NASA POWER data for the year 2024. Figure 3 represents annual trends for air temperature, relative humidity, and global solar radiation in 2024, based on NASA POWER data for the city of Parma.

As in Figure 3, the greatest thermal variations can be detected in summer and winter months, and this behavior deeply affects the growth stage of vegetated façades.

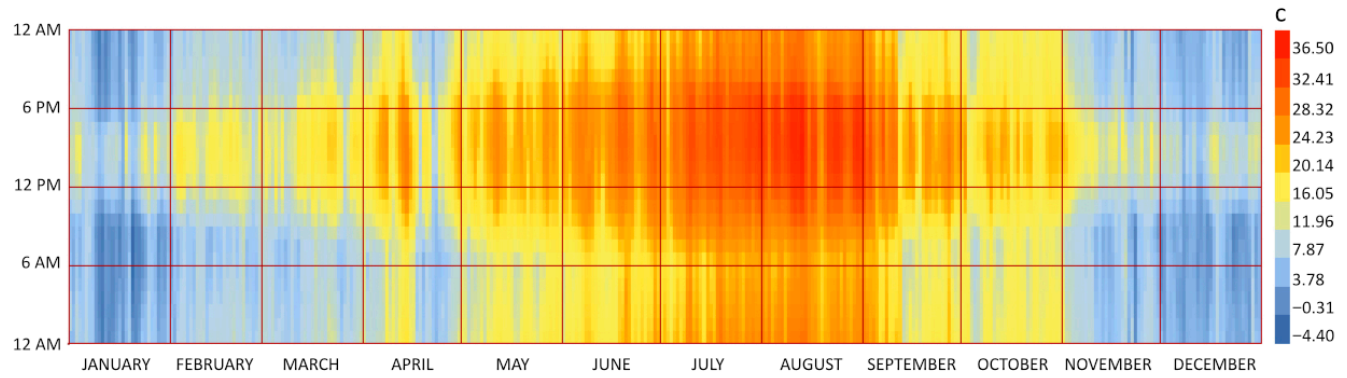


Figure 2. Annual trend of dry-bulb temperature for the year 2024 at the study location (Parma, Italy), based on NASA POWER data.



Figure 3. Air temperature, relative humidity and global solar radiation at the study location (Parma, Italy) based on NASA POWER data.

A comparison between the local weather station and NASA POWER was conducted for four representative weeks—one week each in February, May, July, and October—to assess the seasonal coherence between the two data sources (Figure 4). The results reveal a consistent and physically interpretable pattern of agreement and divergence. In February, the local weather station consistently showed slightly higher daytime maxima (≈1–2 °C) compared with NASA POWER. In May, the datasets show the closest match, with minimal bias and nearly identical diurnal timing. In May, the increasing solar input enhanced the

diurnal temperature range, leading the local station to record moderately higher daytime maxima. In July, the divergence reached its seasonal peak, with the local station exhibiting substantially stronger afternoon heating while maintaining close nighttime agreement. In October, the pattern shifted again, with slightly lower daytime maxima in the local dataset and reduced diurnal amplitude.

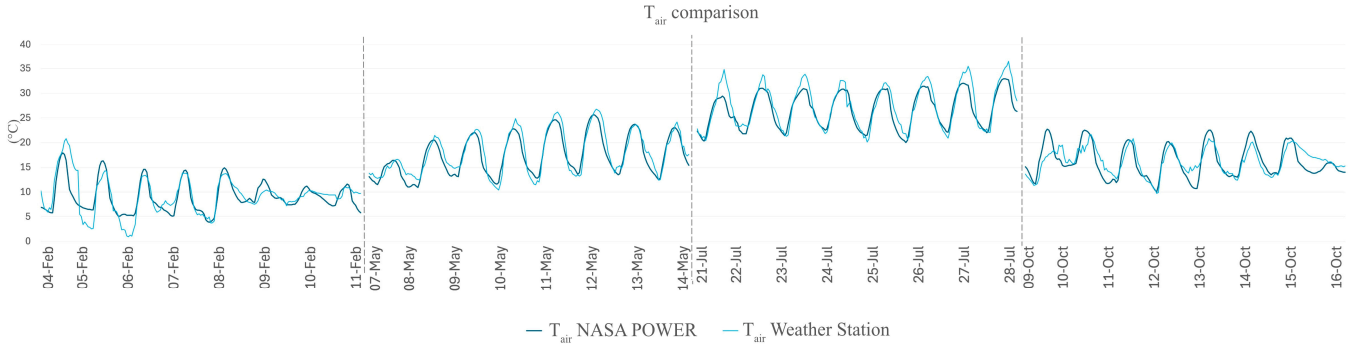


Figure 4. Comparison between local weather station and NASA POWER.

Despite these seasonally dependent differences, both datasets show strong temporal alignment, and NASA POWER demonstrates good overall reliability when evaluated against local observations. Calibration between the local weather station and NASA POWER was carried out to evaluate the consistency and suitability of the datasets prior to their use in subsequent analyses. Such comparison is essential because NASA POWER provides spatially averaged, gridded data, while local stations measure point-scale microclimatic conditions, which can differ substantially, particularly in warm seasons when surface energy processes amplify local variability. Given that the local station is subject to site-specific influences and lacks independent verification, NASA POWER was adopted as the primary reference dataset, with the understanding that the identified seasonal deviations represent inherent differences between point measurements and gridded satellite-derived products.

Operationally, this paper is divided into four main phases:

(i) At first, a microclimate assessment for the base-case building and two different green façades and their immediate surroundings was performed, considering four different weeks, connected to the different LAI values of two plant species, with no reference to higher or lower air temperature peaks.

(ii) The results of each simulation were collected into graphs to compare the thermal behavior of the four assessed weeks, with reference to the leaf area index, LAI, of the selected species and their wall temperatures. In this study, the outdoor air temperature (T_a) and surface-wall temperature (T_0) were used to compare the thermal resilience of the two different green façades on the four different wall orientations.

(iii) The absolute difference of wall temperatures (bare wall and covered wall) was assessed and compared over the year-long period.

(iv) Longwave radiation was considered to evaluate the role of the foliage coverage in reflecting radiation.

(v) Lastly, PET values were considered to evaluate the thermal stress mitigation registered near the vegetated wall to assess the thermal stress resilience potential according to period and wall orientation.

3.1. Materials and Methods

Microclimate assessment for the Cfa climate was carried out using ENVI-met software V5.9.0 to evaluate the thermal performance of a green façade formed by climbing plants growing directly on walls, in the absence of any interposed substrate layers, relative to the base-case condition (a bare wall).

ENVI-met, a three-dimensional microclimate modeling software, was used here to assess and simulate the interactions between urban form, surface materials, vegetation, and atmospheric processes at a very high spatial and temporal resolution.

It was used for microclimatic evaluations by simulating key environmental variables such as air temperature, surface temperature, wind flow, relative humidity, mean radiant temperature, and thermal comfort indices (e.g., PET, UTCI).

ENVI-met is currently the only microclimate simulation software that has been extensively and systematically validated for representing the effects of vegetation on the urban microclimate. Its strength lies in the physically based modeling of plant–atmosphere interactions at multiple scales, from grass and shrubs to trees and vertical greenery systems such as green walls.

The software explicitly simulates key vegetation processes, including shading, evapotranspiration, aerodynamic resistance, leaf area density, and the exchange of heat and moisture between plants, soil, and air. This allows ENVI-met to realistically quantify how different types of vegetation contribute to cooling air and surface temperatures, reducing mean radiant temperature, and improving outdoor thermal comfort [58].

The input data for the ENVI-met model were primarily categorized into four main groups: (i) meteorological data, (ii) vegetation data, (iii) building data, and (iv) thermal comfort data.

i Meteorological data were obtained from NASA POWER for the entire year 2024 to enable a full forcing evaluation. Simulations were performed for four distinct periods, each spanning 168 h (seven days), corresponding to representative stages of vegetation growth rather than extreme temperature conditions. Considering the complete annual growth cycle of the two selected climbers, four weeks were identified as representative of seasonal variations in leaf area index (LAI), as illustrated in Figure 2 for *Hedera helix* and *Parthenocissus tricuspidata*.

ii With regard to the botanical data [40,45,49] (Figure 5), the first selected week (Period A: 4–11 February 2024) corresponded to the minimum LAI for Parthenocissus tricuspidata (approximately 0.40), indicating a stage with minimal foliage, while Hedera helix maintained an average LAI of 3.72. Period B (7–14 May 2024) showed an inverted trend, with Parthenocissus tricuspidata initiating its new foliage season and reaching a higher LAI value of approximately 4.30, while the LAI of Hedera helix remained stable at around 3.66. The third period (21–28 July 2024) registered the lowest LAI values (2.78) for Hedera helix, despite the plant being an evergreen climber. During the hottest season, its LAI decreased, whereas Parthenocissus tricuspidata reached its maximum foliage density, with an LAI of approximately 4.80. The fourth period (9–16 October 2024) showed a decrease in LAI for Parthenocissus tricuspidata as it began to shed its leaves, reducing its LAI to approximately 3.90. In contrast, Hedera helix exhibited an increase in LAI, reaching about 4.29. The building models were assumed to have all four façades fully covered with vegetation, as adopted in previous studies [59], to represent a fully grown scenario.

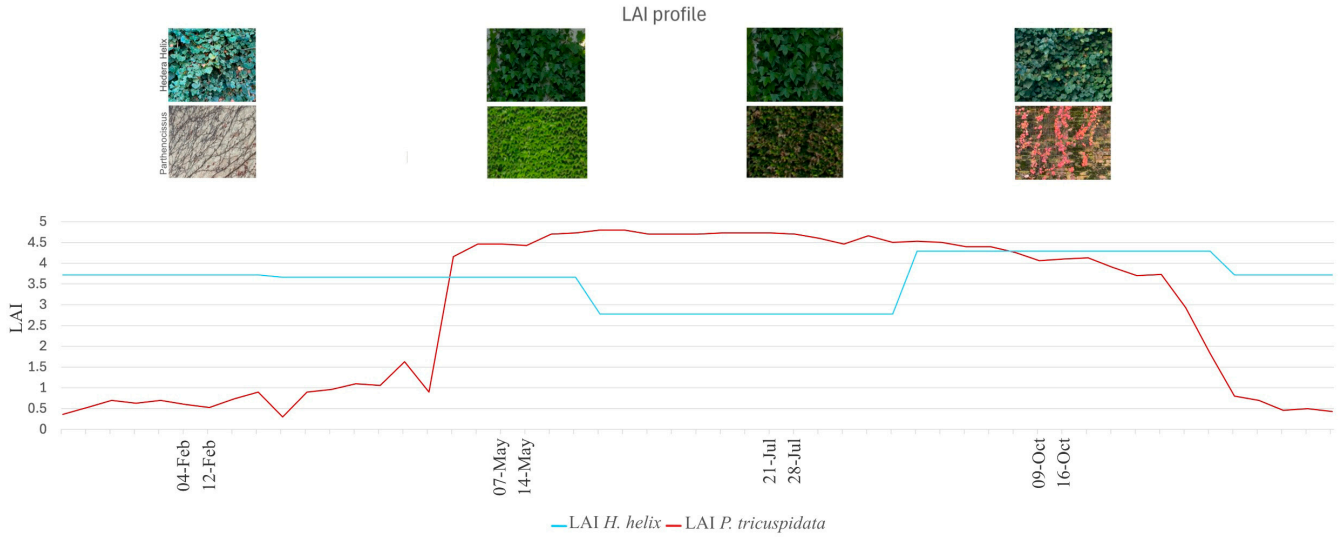


Figure 5. Average LAI values for *Parthenocissus tricuspidata* and *Hedera helix*.

Moreover, additional botanical data for the LAI [60], albedo [61,62], and emissivity [63] of both species were averaged for each selected weekly period based on the literature and served as representative input conditions for the plant growth cycles of *Hedera helix* and *Partenocissus tricuspidata*, as depicted in Table 1. This approach was necessary because LAI, albedo, and emissivity are highly sensitive to meteorological conditions—such as sky state and the availability of photosynthetically active radiation—which strongly influence plant transpiration and overall foliage behavior. In Table 1, the values are compared with those obtained through a direct destructive method, in which the authors collected all leaf material from sample plants [64]. The evaluation of LAI for both *P. tricuspidata* and *H. helix* was performed by measuring the average leaf area over a 1 m^2 sample and relating it to 1 m^2 of façade surface. Due to the complexity involved in accurately calculating LAI, the literature-based values are preferred for comparative numerical evaluation.

Table 1. Botanical data used in the ENVI-met simulations for *Parthenocissus tricuspidate* and *Hedera Helix*.

Period	Simulation Date	LAI *P. tricuspidata* (*)	LAI *H. helix* (*)	Average Albedo *P. tricuspidata* **	Average Albedo *H. helix* **	Emissivity *P. tricuspidata*	Emissivity *H. helix*
A	4–11 February 2024	0.40 (0.48)	3.72 (3.73)	0.30	0.20	0.95	0.97
B	7–14 May 2024	4.30 (4.48)	3.66 (3.65)	0.22	0.20	0.95	0.97
C	21–27 July 2024	4.80 (4.90)	2.78 (2.90)	0.22	0.20	0.95	0.97
D	9–16 October 2024	3.90 (4.03)	4.29 (4.23)	0.18	0.20	0.95	0.97

** The color represents the average leaf coloration observed during the corresponding period. (*) represents the sample measured values on site.

In addition to LAI values for the two climber species, particular attention was given to average albedo and leaf emissivity. Albedo is of special interest because it reflects seasonal variations in foliage color. For *Parthenocissus tricuspidata*, changes in leaf color significantly influence albedo: during the growing stage, leaves are predominantly light green, with albedo values around 0.22; in autumn, the foliage turns reddish, reducing albedo to approximately 0.18; and in winter, it increases to about 0.30. In contrast, *Hedera helix*, being an evergreen species, maintains a relatively constant albedo of approximately 0.20 throughout the year. In this first attempt to evaluate the role of climbing species, stomatal conductance has been deliberately overlooked, even though valuable attempts to use the ENVI-met model to assess and calculate transpiration through stomatal resistance are available [64]. Currently, ENVI-met provides two methods for estimating stomatal resistance: a simple approach based on the work of Deardorff [65] and the A-gs model [66].

The Deardorff approach scales a prescribed maximum stomatal resistance according to solar radiation input and water availability, whereas the A-gs model computes plant photosynthetic activity and derives the corresponding CO_2 demand, from which the stomatal state is subsequently inferred.

iii The building model and simulation settings are summarized in Table 2. Wall and roof material properties were derived from the default ENVI-met database to represent a non-specific building envelope, considered representative of typical U-values and construction characteristics commonly found in buildings located in the northern Italian climate. Soil temperature was estimated using default values and relevant data from the literature. The simulation domain was defined as 9 m × 9 m × 4 m, with a grid resolution of 1 m × 1 m × 1 m. Meteorological boundary conditions were set to full forcing, and each simulation covered a 168 h period (seven days). Additional grid resolutions (2 m × 2 m × 2 m and 3 m × 3 m × 3 m) were also tested; however, no appreciable differences were observed, while computational time increased unnecessarily.

Table 2. Simulation setting data used for the ENVI-met simulations.

Simulation area	44°48′05.3″ N; 10°19′40.8″ E
Köppen–Geiger classification	Cfa
Modeling area domain	9 m × 9 m × 4 m
Grid dimension	1 m × 1 m × 1 m
Meteorological boundary condition	Full forcing
Simulation duration for each period (h)	168 h
Simulation starting time	05:00 a.m.
Thickness of vegetation layer (ΔC)	0.10 m
Air gap size between substrate and building wall (ΔAG)	0.00 m

Three building configurations were tested:

- Base case: façade without vegetation (Figure 6a).
- *Hedera helix*: façade covered with *Hedera helix* on all orientations, growing directly on the wall (Figure 6b).
- *Parthenocissus tricuspidata*: façade covered with *Parthenocissus tricuspidata* on all orientations, growing directly on the wall (Figure 6b).



Figure 6. Building model used as the base case (**a**) and for the green façade sample building (**b**).

All scenarios were compared to the base case, considering all four wall orientations.

Default values (Table 3) were assumed in the ENVI-met configuration, representing averaged parameters typical of building envelopes in Cfa climates, including the presence of a scarce layer of insulation material, as adopted in previous studies [67]. Since different

building materials can influence thermal performance, the objective of this study is to isolate and compare the relative thermal behavior of different green façade configurations under consistent boundary conditions by adopting standard and fixed wall layers, as in Table 3.

Table 3. Building material properties used for the ENVI-met simulations.

Material	Thermal Conductivity	Emissivity	Absorption	Transmission	Reflection
Default plaster	0.6	0.93	0.60	0.00	0.40
Default insulation	0.07	0.90	0.50	0.00	0.50
Default concrete	1.6	0.90	0.70	0.00	0.30

iv In outdoor thermal comfort research, the Physiological Equivalent Temperature (PET) and the Universal Thermal Climate Index (UTCI) are among the most widely used indicators [68,69]. UTCI is based on Fiala's multi-node thermoregulation model [70], which relates the physiological effects of complex thermal environments on the human body to those observed under a standardized air temperature (Ta), emphasizing stress prediction under extreme conditions [71]. Conversely, PET is derived from the Munich Energy Balance Model for Individuals (MEMI) using a two-node approach [72]. It represents the air temperature at which, in a typical indoor setting, the human heat budget is balanced with the same core and skin temperatures as those under the outdoor conditions being assessed. Namely, the PET defines all incoming and outgoing fluxes in the human body; therefore, PET is considered a robust biometeorological parameter because it links physical environmental variables to human thermal perception [73], also involving MRT values. Based on PET's ability to effectively quantify the relationship between MRT reduction and heat stress levels under different vegetation configurations, PET was selected as the most reliable metric for this study. The calculation of PET requires air temperature, humidity, wind speed, and radiation as input parameters. In this study, PET was computed using ENVI-met software, which, according to the BIO-met model, considers a 35-year-old man with average physiological characteristics. ENVI-met calculates PET values using 3D vegetation models that incorporate plant physiological properties as well as leaf-level characteristics. In addition, ENVI-met applies a complex ray-tracing algorithm to quantify shading (i.e., the reduction in incident solar radiation) and to model longwave radiation exchanges within the vegetation canopy, which constitute primary drivers of PET reduction.

The model computes leaf-surface temperatures by solving the leaf energy-balance equation, explicitly accounting for transpiration rates. Transpiration contributes to cooling by lowering the air temperature in the canopy layer, as determined by the species-specific physiological behavior of the plants. Finally, the BIO-met module uses the resulting meteorological fields to calculate PET, integrating human-related parameters such as activity level and clothing insulation.

3.2. ENVI-Met Setup and Green Façade Calculation

ENVI-met has been demonstrated [74] to be the most sophisticated and reliable software in evaluating the complex vegetation–atmosphere feedback mechanisms by dynamically linking stomatal responses to humidity fields [75]; furthermore, it provides cross-seasonal adaptability via its Tree Calendar function, which aligns leaf area senescence with radiative transfer processes [58].

The ENVI-met software incorporates an integrated plant database that offers comprehensive information on a variety of plant species, enabling users to simulate and analyze the impacts of different vegetation types on urban microclimates [76].

In ENVI-met, stomatal conductance and transpiration are parameterized within the plant profile (namely the *P. tricuspidata* and *H. helix* data) using a biological, process-based approach. ENVI-met is able to model the exchange of CO_2 and water vapor at the leaf level using an adaptation of Jacobs' A−gs stomata model [66]. The A−gs model is used to estimate the stomatal behavior of single leaves, taking into account the microclimatic conditions of the whole plant. In this model, it is assumed that plants operate stomatal conductance in a way that maximizes CO_2 gain, while associated water loss is minimized. As an empirical model, the A−gs model links stomatal conductance (water loss) with photosynthesis (CO_2 gain). Empirical studies have found a strong correlation between the stomatal conductance of water and photosynthesis. Using this relation, the calculation of net photosynthesis rates allows the model to calculate the stomatal behavior of a plant. Recent studies [76] indicate that ENVI-met is capable of simulating the transpiration rates and leaf temperatures of trees in both building and urban environments.

Figure 7 illustrates the conceptual representation of a green façade in ENVI-met, highlighting key variables at the interface with the atmosphere (air temperature, Ta) and within the green layer (canopy air temperature, TaC). The node T_0 represents the surface temperature of the outermost wall layer and serves as the primary reference point for evaluating heat exchange between the wall and the external environment [77].

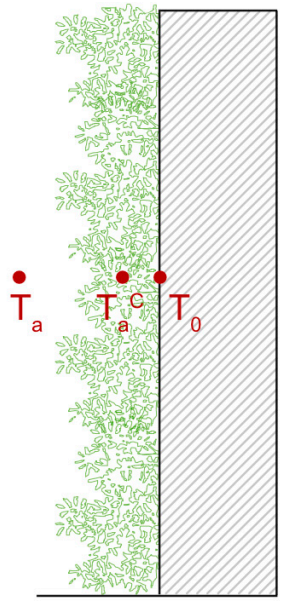


Figure 7. Conceptual diagram of a green wall system with a greening layer, illustrating the main variables (adapted from the ENVI-met manual).

Within ENVI-met, the transfer of longwave radiation through and within the vegetative layer is not modeled using explicit transmission coefficients. Instead, the approach incorporates a probabilistic parameter, referred to as coefficient P (Figure 8), which quantifies the likelihood that incident longwave radiation will be intercepted by the leaf surface.

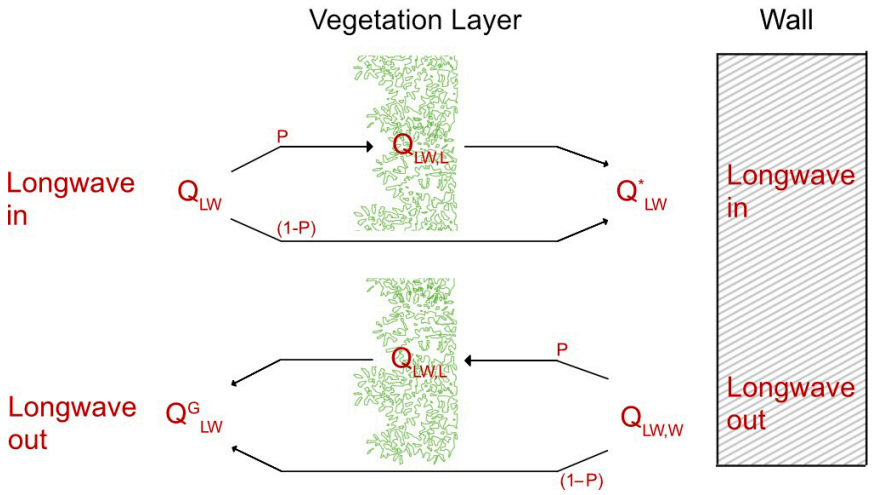


Figure 8. Longwave radiation scheme as calculated in ENVI-met (adapted from the ENVI-met manual).

The change in longwave radiation behind the plant layer (Q^{*}_{LW}) can be calculated as a weighted average between the incident longwave radiation (Q_{LW}) and that emitted by the leaves ($Q_{LW,L}$):

$$Q^{*}_{LW} = (1 - P)\, Q_{LW} + P\, Q_{LW,L} \quad (1)$$

The total emission of longwave radiation from the façade ($Q_{G,LW}$) follows a similar principle, combining the radiation emitted by the leaves and that emitted by the wall surface:

$$Q_{G,LW} = P\, Q_{LW,L} + (1 - P)\, Q_{LW,W/S} \quad (2)$$

Analyzing longwave radiation outcomes in ENVI-met requires evaluating how vegetation modifies the thermal radiation emitted by building surfaces relative to a bare façade. In vegetated configurations, shading and evapotranspiration lower the wall-surface temperature, which in turn reduces the magnitude of longwave radiation emitted toward the surrounding environment.

This attenuation of radiative heat release reflects the capacity of green façades to moderate surface thermal loads and contributes to a reduction in nearby temperatures.

Lastly, attention should be given to the role of irrigation. In ENVI-met, it is assumed that a managed irrigation system is available to support plant growth and maintain an adequate water supply.

To represent this, an adjustable watering coefficient (ζw) is defined, ranging from 0 (dry conditions) to 1 (moist conditions), indicating the level of water accessibility for plants. For green façade systems without a substrate layer (e.g., climbing plants, as in this research), ENVI-met assumes a constant and sufficient water supply ($\zeta w = 1$).

4. Results

4.1. Wall Temperature T_0

The first set of results involved a comprehensive analysis of the T_0 profiles together with the absolute difference profiles. Figure 9 illustrates the T_0 trends for each orientation, accounting for the seasonal variability of the leaf area index (LAI) of both species, with the objective of evaluating the influence of vertical greenery on the thermal performance of the façade compared to the reference condition (bare wall). Figure 10 presents the absolute difference profiles for each period and orientation. All four periods span 168 h, starting at 06:00 on the first day and ending at 06:00 on the last day, thereby ensuring a consistent temporal framework for comparison.

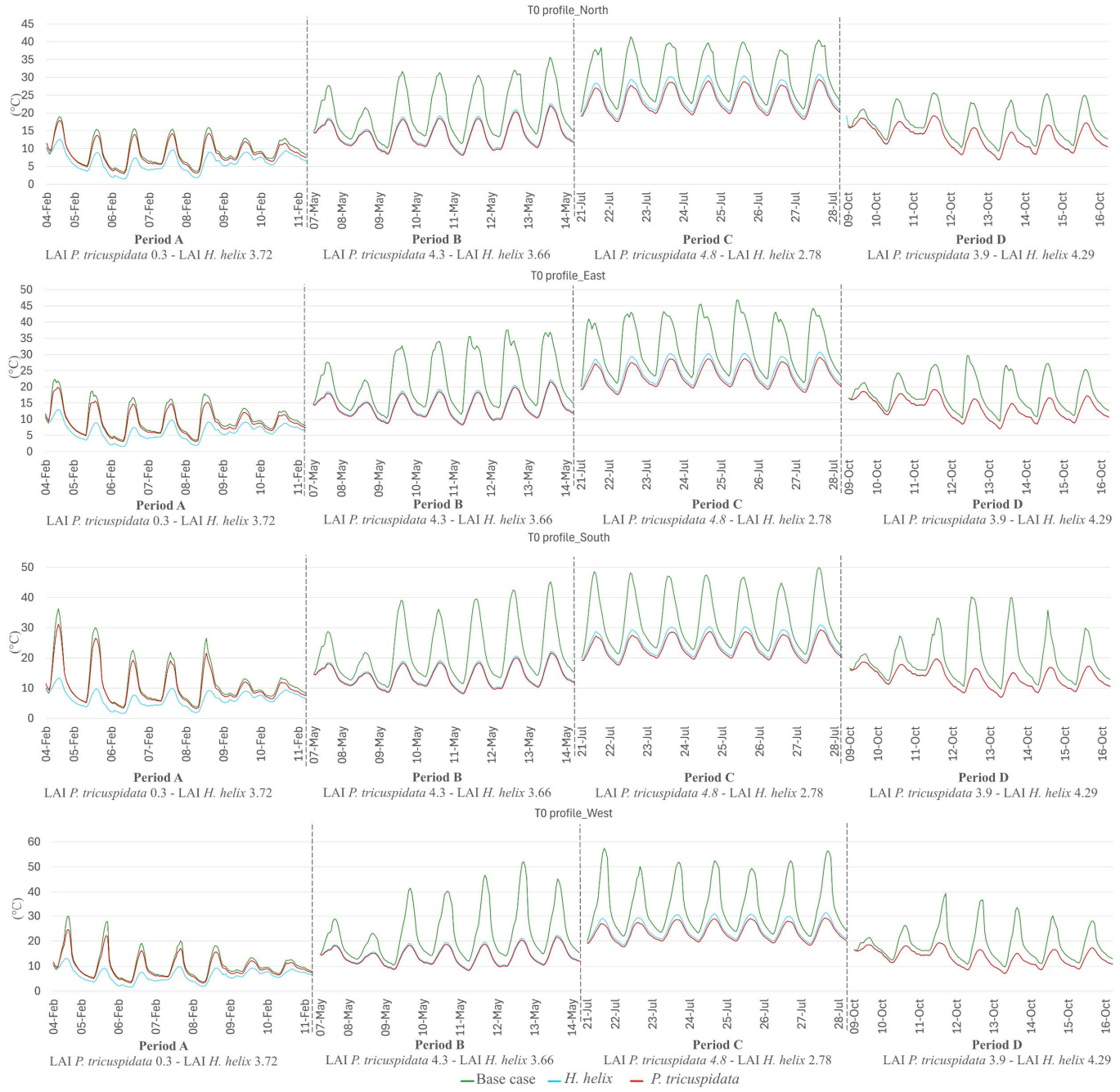


Figure 9. T_0 profile for the four wall orientations, with reference to four different periods.

During Period A (11 February), *Parthenocissus tricuspidata* showed the lowest LAI (0.30), whereas *Hedera helix* attained its annual maximum (3.72).

On the north façade, *P. tricuspidata* is associated with the lowest nighttime T_0, with a minimum of 1.8 °C on 8 February, consistent with values recorded on the bare wall (3.6 °C) and on *H. helix* (3.1 °C). The highest north-facing temperatures occurred on the first day of the week. During the daytime, the bare wall reached 18.7 °C, slightly higher than *H. helix* (17.7 °C at noon). The bare wall thermal range spanned 18.7–3.6 °C, while *H. helix* showed a narrower range (17.7–3.1 °C), indicating comparable thermal behavior. The maximum absolute difference was observed for *H. helix* at the mid-period (8.0 °C), whereas *P. tricuspidata* exhibited a markedly lower maximum difference (1.6 °C) on the same day.

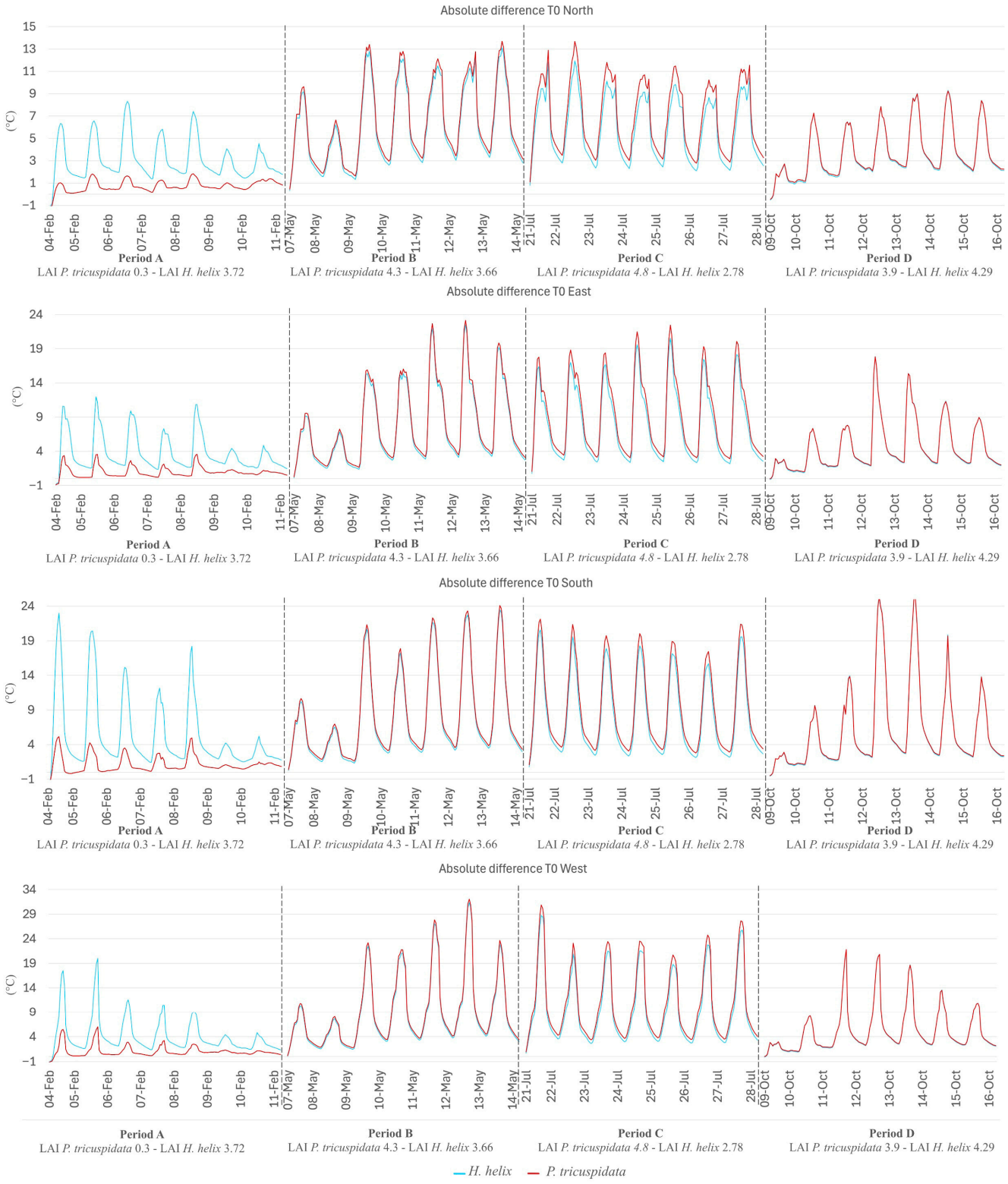


Figure 10. Absolute difference T_0 for the four wall orientations, with reference to four different periods.

On the east façade, the bare wall T_0 showed two daytime peaks (12:00–14:00) on 4, 5, 7, and 8 February, with a maximum of 22.3 °C on the first day (~12:00). On 5 February, an initial peak of 18.7 °C was followed by a slight dip and a second rise to 17.4 °C at 14:00. *P. tricuspidata* displayed a more regular pattern, with peaks aligned to midday and a maximum of 19.3 °C at 15:00—about four hours after the bare wall. With higher LAI, *Hedera helix* shows lower averages; its maximum was 13.0 °C at 14:00 on 4 February, one

hour after the peaks observed for the bare wall and *P. tricuspidata*, and its minimum was 1.9 °C at 07:00 on 8 February. In absolute difference (Figure 10), *H. helix* reached an average maximum peak of 8.2 °C, with the highest value being 11.2 °C on 5 February at 13:00; in the same interval, *P. tricuspidata* showed its largest deviation of 3.5 °C.

On the south façade, the bare wall attained its maximum on 9 February at 14:00 (36.3 °C), then declined. *P. tricuspidata* followed the same pattern, peaking at 31.1 °C due to seasonal leaf absence. *H. helix* reached 13.3 °C on the same date and hour. The lowest temperatures occurred on 8 February, coinciding with the 2024 air-temperature minimum (mean 4.7 °C at 08:00). At that time, T_0 was 3.8 °C at the bare wall, 3.3 °C with *P. tricuspidata*, and 1.9 °C with *H. helix*. In terms of the absolute difference, the south façade showed the largest reductions vs. the bare wall: 23.0 °C on the first day, then decreasing from 20.3 °C to 18.2 °C and finally to 5.2 °C, which was close to *P. tricuspidata*. For *P. tricuspidata*, the maximum coincided with *H. helix's* peaks (5.1 °C), with a more homogeneous weekly trend.

On the west façade, bare-wall T_0 peaks coincided with *P. tricuspidata* but were ~5.0 °C higher (29.8 °C and 29.8 °C at 15:00–16:00 vs. 24.5 °C and 24.4 °C). Mid-period, bare-wall maxima ranged from 20.9 to 17.4 °C, with *P. tricuspidata* ~2.0 °C lower. *H. helix* remained markedly cooler and peaked earlier (typically 14:00), with absolute maxima of 12.9 °C on 4 February (14:00) and 9.6 °C on 7 February; the minimum was 1.7 °C at 07:00 on 6 February. In terms of the absolute difference (Figure 10), day two of Period A showed the greatest deviations: 20.0 °C for *H. helix* and 6.0 °C for *P. tricuspidata*. Overall, *H. helix* differences were largest at the beginning, then progressively flattened.

During Period B (7–14 May), *Hedera helix* showed a slightly lower LAI (3.66) than in winter, despite this being a counterintuitive seasonal trend, whereas *Parthenocissus tricuspidata* increased markedly to an LAI of 4.30.

On the north façade, increasing air temperature drove a corresponding rise in bare-wall T_0, reaching a daytime maximum of 35.0 °C and a nocturnal minimum of 10.1 °C, indicating a large diurnal amplitude, despite limited direct radiation. The two climbers displayed largely comparable thermal trajectories due to similar LAI values. Maximum T_0 values were recorded on 13 May at 16:00 (22.5 °C for *H. helix*; 21.9 °C for *P. tricuspidata*), while minima occurred at 06:00 (8.4 °C and 8.1 °C, respectively); the bare wall reached its minimum at 05:00 (11.4 °C). In terms of absolute difference (Figure 10), both climbers showed similar trends, with inter-species deltas below 1.0 °C, although *P. tricuspidata* exhibited slightly larger differences relative to the bare wall. Peak reductions occurred in the second half of the week, with maxima on 14 May (13.7 °C and 12.9 °C).

On the east façade, the second half of the week reproduced Period A's pattern, with two daily T_0 peaks: a first peak between 12:00 and 13:00 (36.8–36.3 °C), followed by a decline and a second maximum of 36.8 °C. A similar behavior was observed on the bare wall. In contrast, *H. helix* and *P. tricuspidata* exhibited smoother profiles, peaking between 15:00 and 16:00. The two species showed comparable behavior, with *H. helix* consistently ~1.0 °C warmer than *P. tricuspidata*, and a day–night thermal amplitude of ~8.0 °C. Absolute differences relative to the bare wall were nearly identical for both climbers (Figure 10), with maximum values in the second half of the period (23.1 °C for *P. tricuspidata*; 22.4 °C for *H. helix*). A secondary peak occurred approximately two hours later in both profiles.

On the south façade, bare-wall temperature increased from 7 May, reaching a maximum of 45.0 °C on 13 May at 15:00; the minimum occurred at 05:00 on 9 May (10.2 °C). The thermal profiles of *P. tricuspidata* and *H. helix* were nearly identical, with mean daily temperatures differing by <0.1 °C. Peak values for both climbers coincided with the bare-wall maximum (13 May, 15:00), reaching 22.2 °C for *H. helix* and 21.5 °C for *P. tricuspidata*. Absolute differences show comparable trends for the two species, with minimal inter-species

variability; *P. tricuspidata* exhibited a slightly larger reduction relative to the bare wall. The absolute difference between the climbers remains approximately 0.5 °C.

On the west façade, a pattern similar to that of the east façade was observed. After relatively low temperatures during the first two days, the bare wall peaked at 52.1 °C on 13 May at 18:00. Under dense foliage, both *H. helix* and *P. tricuspidata* showed comparable trends, peaking concurrently at 18:00 with T_0 values of 20.7 °C and 20.0 °C, respectively, indicating a substantial attenuation of peak temperatures. Nighttime minima differed less markedly, with an average gap of ~5.0 °C between the bare wall and vegetated façades. Unlike Period A, absolute differences in Period B were slightly larger for *P. tricuspidata*, which reached a maximum of 32.0 °C compared to 31.0 °C for *H. helix*.

During Period C (21–28 July), *Parthenocissus tricuspidata* attained its annual maximum LAI (4.80), whereas *Hedera helix*, affected by high air temperatures influencing evapotranspiration, showed its lowest LAI (2.78).

On the north wall, bare-wall T_0 peaked at 41.4 °C at 14:00 on 22 July, the hottest week of 2024 (air temperature ~31.0 °C, NASA POWER). At the same time, *H. helix* reached 29.5 °C, while *P. tricuspidata* peaked slightly later at 27.7 °C (15:00). The lowest nocturnal temperatures also occurred on 22 July at 02:00 (bare wall 23.0 °C, *H. helix* 19.7 °C, and *P. tricuspidata* 19.0 °C). Absolute differences relative to the bare wall were consistently greater for *P. tricuspidata*, with a maximum reduction of 13.7 °C (vs. 11.9 °C for *H. helix*), persisting throughout the week, including at nighttime.

On the east façade, the bare wall showed a stable pattern over the 168 h period, with two daily peaks separated by ~2 h: 42.2–42.5 °C between 12:00 and 13:00, followed by a second maximum of 43.0 °C at 15:00. In contrast, both climbers exhibited a single daily peak at 14:00 (28.5 °C for *H. helix*; 26.8 °C for *P. tricuspidata*), with average maxima of 29.8 °C and 28.1 °C, respectively. Minimum temperatures ranged from 17.7 to 20.0 °C for *P. tricuspidata* and reached 18.4 °C for *H. helix*. Absolute difference profiles (Figure 10) mirrored those of the north façade, with *P. tricuspidata* achieving the largest reductions (22.4–17.8 °C), and *H. helix* with slightly lower values (19.8–16.4 °C).

On the south façade, bare-wall peak temperatures fluctuated between 49.9 °C and 44.8 °C. Both climbers closely follow the bare-wall trend, with the largest peak reductions on 27 July (19.6 °C for *H. helix*; 21.8 °C for *P. tricuspidata*). The greatest absolute differences occurred at the beginning and end of Period C, when *P. tricuspidata* reached 22.1 °C and 21.3 °C, respectively, while *H. helix* ranged from 20.6 °C to 19.4 °C. The minimum reduction for *H. helix* was observed on 26 July (15.8 °C).

On the west façade, central-day peaks remained near 50.0 °C, except for maxima on 21 July (57.4 °C) and 28 July (55.7 °C). Nocturnal minima occurred at 06:00–07:00, ranging from 22.0 °C to 23.5 °C. Both climbers showed similar thermal evolutions: *H. helix* peaked at 30.7 °C on 25 July at 16:00 and dropped to 18.7 °C on 22 July at 05:00, while *P. tricuspidata* reached 28.5 °C on the same day and a minimum of 18.0 °C at 05:00 on 22 July. The largest absolute differences occurred on 21 and 28 July, with *P. tricuspidata* reaching 30.8 °C and 27.8 °C, exceeding those of *H. helix* (28.1 °C and 25.9 °C).

During Period D (9–16 October; Figure 8), the two climber species exhibited similar thermal behaviors, reflecting comparable LAI values (4.29 for *Hedera helix* and 3.90 for *Parthenocissus tricuspidata*).

On the north façade, bare-wall temperature variability was lower than in Periods B and C, with a maximum of 26.7 °C (11 October, 13:00) and a minimum of 11.1 °C (13 October, 03:00). Vegetated façades showed coincident peaks on 11 October at 14:00 (19.2 °C for *H. helix*; 19.2 °C for *P. tricuspidata*), confirming nearly identical performance. Absolute differences were variable; however, except for the first day, the largest daily

reductions were associated with *P. tricuspidata*, typically ~8.0 °C below the bare wall, with a similar pattern for *H. helix*.

On the east façade, the bare wall exhibited heterogeneous behavior, peaking before noon (29.6 °C at 11:00 on 12 October) and reaching a minimum of 9.4 °C at 08:00 on 13 October. Both climbers reached nearly identical maxima at 14:00 on 13 October (19.2 °C for *H. helix*; 19.2 °C for *P. tricuspidata*). Minima coincided with the bare wall but were lower (7.0 °C vs. 9.4 °C at 08:00). Absolute differences (Figure 10) were identical for both species, increasing from 6.6–7.5 °C at the start of the week to a maximum of 17.8 °C on 13 October, then decreasing to 11.3–8.6 °C toward the end.

On the south façade, bare-wall T_0 increased progressively, reaching peak values of 40.0 °C at 15:00 on two consecutive days, while the minimum (9.7 °C) occurred on 13 October at 08:00. Vegetated façades peaked between 15.2 °C and 19.2 °C at the same hour, with minima at 08:00 on 13 October (7.0 °C for *H. helix*; 6.9 °C for *P. tricuspidata*), confirming substantial thermal attenuation during the transitional season. Absolute differences peaked on the two central days (~25.0 °C for both species) and reached a minimum on 10 October (~1.0 °C).

On the west façade, the bare-wall T_0 was highly variable, peaking at 39.3 °C on 11 October at 18:00 and reaching a minimum of 9.6 °C at 08:00 on 13 October. Both climbers exhibited nearly identical profiles, with minima coincident with the bare wall but ~7.0 °C lower. Their maxima occurred earlier than that of the bare wall (11 October, 14:00), reaching 19.2 °C for both species, indicating a time lag in the thermal response of vegetated façades. Absolute differences peaked at 21.8 °C on 11 October and decreased to 10.7 °C by the last day.

According to Table 4, the largest temperature reduction relative to the bare wall for the *Hedera helix*-covered façade occurred on the west orientation during Period B, specifically on 12 May, with a peak difference of 31.3 °C between 09:00 and 17:00 (8 h). For *Parthenocissus tricuspidata*, the maximum T_0 reduction was observed on the same day and within the same interval, reaching 32.0 °C.

Table 4. Wall temperature (T_0) for the four wall orientations across four seasonal periods, comparing the reference configuration (bare wall) with vegetated façades covered by *H. helix* and *P. tricuspidata*.

Period	Orientation	Base Case	*Hedera helix*				*Parthenocissus tricuspidata*			
		T_0 Range from 9 am to 5 pm (°C)	**T_0 Range from 9 am to 5 pm (°C)**	**Max °T Reduction (°C)**	**Date with Maximum °T Reduction**	**Time with °T Reduction > 10 °C (Duration/h)**	**T_0 Range from 9 am to 5 pm (°C)**	**Max °T Reduction (°C)**	**Date with Maximum °T Reduction**	**Time with °T Reduction > 10 °C (Duration/h)**
A	North	4.5–18.9	1.6–12.6	8.3	6 February	/	3.8–17.9	1.8	8 February	/
	East	5.0–22.3	1.7–13.0	11.9	5 February	11:00–12:00 (1)	4.2–19.9	3.6	8 February	/
	South	5.1–36.3	1.7–13.3	23.0	4 February	11:00–17:00 (6)	4.34–31.2	5.1	4 February	/
	West	4.7–29.8	1.7–13.0	20.0	5 February	11:00–17:00 (6)	4.0–24.5	5.9	5 February	/
B	North	15.4–35.6	12.0–22.5	13.1	13 May	11:00–17:00 (6)	11.5–22.0	13.7	13 May	10:00–17:00 (7)
	East	15.3–37.6	12.3–22.1	22.4	12 May	09:00–17:00 (8)	11.7–21.5	23.1	12 May	09:00–17:00 (8)
	South	15.4–45.2	11.9–22.2	23.5	13 May	09:00–17:00 (8)	11.4–21.5	24.1	13 May	09:00–17:00 (8)
	West	15.4–52.1	11.8–22.2	31.3	12 May	09:00–17:00 (8)	11.3–21.5	32.0	12 May	09:00–17:00 (8)
C	North	27.4–41.4	22.0–30.9	11.9	22 July	12:00–16:00 (4)	21.0–29.4	13.7	22 July	11:00–17:00 (6)
	East	35.6–46.8	22.4–30.7	20.5	25 July	09:00–16:00 (7)	21.1–39.1	22.4	25 July	09:00–17:00 (8)
	South	28.7–49.9	21.9–30.9	20.5	21 July	10:00–17:00 (7)	20.9–29.2	22.1	21 July	10:00–17:00 (7)
	West	26.9–57.4	21.8–31.3	28.7	21 July	13:00–17:00 (4)	20.9–29.2	30.8	21 July	13:00–17:00 (4)
D	North	13.2–25.7	8.5–19.2	9.3	14 October	/	8.4–19.2	9.2	14 October	/
	East	16.3–29.6	8.7–19.2	17.9	12 October	09:00–13:00 (4)	8.7–19.2	17.8	12 October	09:00–13:00 (4)
	South	16.3–40.2	8.6–19.5	25.8	13 October	10:00–17:00 (7)	8.5–19.6	25.6	13 October	10:00–17:00 (7)
	West	13.1–39.3	8.5–19.2	21.8	11 October	09:00–17:00 (8)	8.5–19.2	21.8	11 October	09:00–17:00 (8)

The smallest T_0 differences were recorded during Period A, when *H. helix* reduced north façade temperatures by 8.3 °C, whereas *P. tricuspidata*, in the absence of foliage, achieved only a 1.8 °C reduction.

Time intervals with temperature reductions exceeding 10.0 °C occurred for *H. helix* during Period B on the south, east, and west façades, persisting for more than eight consecutive hours. A comparable behavior was observed for *P. tricuspidata*, where T_0 remained reduced for over eight hours.

Post-sunset thermal behavior was analyzed for each orientation across the four periods to assess the thermal lag of the bare wall relative to the vegetated façades. Table 5 reports mean, maximum, and minimum differences between the bare and green façades, considering period-specific sunset times to ensure consistent post-sunset comparisons.

Table 5. Difference in T_0 (°C) after sunset between the bare wall and the two green façade configurations, *Hedera helix* and *Parthenocissus tricuspidata*.

		Hedera helix			***Parthenocissus tricuspidata***		
		Average T_0 Diff (°C)	**Max T_0 Diff (°C)**	**Min T_0 Diff (°C)**	**Average T_0 Diff (°C)**	**Max T_0 Diff (°C)**	**Min T_0 Diff (°C)**
A	North	2.8	5.5	1.7	0.7	1.4	0.1
	East	3.1	5.8	1.9	0.7	1.3	0.2
	South	4.0	14.4	1.7	0.7	2.1	−0.2
	West	4.4	20.0	1.9	1.1	0.2	0.2
B	North	4.3	7.3	1.8	4.7	7.7	2.2
	East	4.3	6.4	1.9	4.7	6.8	2.2
	South	4.6	7.2	1.8	5.0	7.6	2.2
	West	6.2	13.3	2.2	6.6	13.7	2.5
C	North	3.9	5.0	3.0	4.8	5.8	3.8
	East	4.1	4.6	3.3	4.9	5.5	4.1
	South	4.3	5.2	3.1	5.2	6.0	3.9
	West	6.3	8.8	4.7	7.2	9.8	5.6
D	North	2.7	4.8	0.9	2.9	4.8	1.1
	East	3.0.	5.5	1.0	3.1	5.5	1.1
	South	3.8	8.4	1.0	3.9	8.4	1.1
	West	4.0	9.7	1.0	4.1	9.7	1.1

Suset hours: Period A: 17:31–17:41; Period B: 20:19–20:25; Period C: 20:50–20:57; Period D: 18:33–18:45.

During Period A (sunset between 17:31 and 17:41), *H. helix* exhibited the highest post-sunset temperature difference, reflecting limited thermal variability. The presence of *H. helix* moderated cooling, reducing exposure to cold air and maintaining more homogeneous wall temperatures over the diurnal cycle.

By contrast, *P. tricuspidata* showed a thermal response similar to the bare wall during Period A, owing to the absence of foliage, resulting in negligible average differences. The maximum mean post-sunset temperature difference between the bare wall and *H. helix* was observed during Period C (sunset between 20:50 and 20:57) on the west façade (6.3 °C). Under the same conditions, *P. tricuspidata* reached its highest post-sunset difference (7.2 °C), associated with its maximum LAI and enhanced shading and thermal buffering.

4.2. Longwave Radiation

The second stage of the analysis examined longwave radiation emitted and received by the different façade configurations (Figure 11).

During Period A, the bare wall recorded received longwave radiation of 293–369 W m^{-2}, while emitted radiation ranged from 331 to 508 W m^{-2} on the south and west façades and from 329 to 426 W m^{-2} on the north and east façades. Vegetated façades exhibited substantially higher values: *Hedera helix* recorded a received radiation of 616–735 W m^{-2} and emitted radiation of 629–766 W m^{-2} across all orientations. On the south façade, *Parthenocissus tricuspidata* exceeded both *H. helix* and the bare wall, with a received radiation of 629–833 W m^{-2} and emitted radiation of 641–832 W m^{-2}.

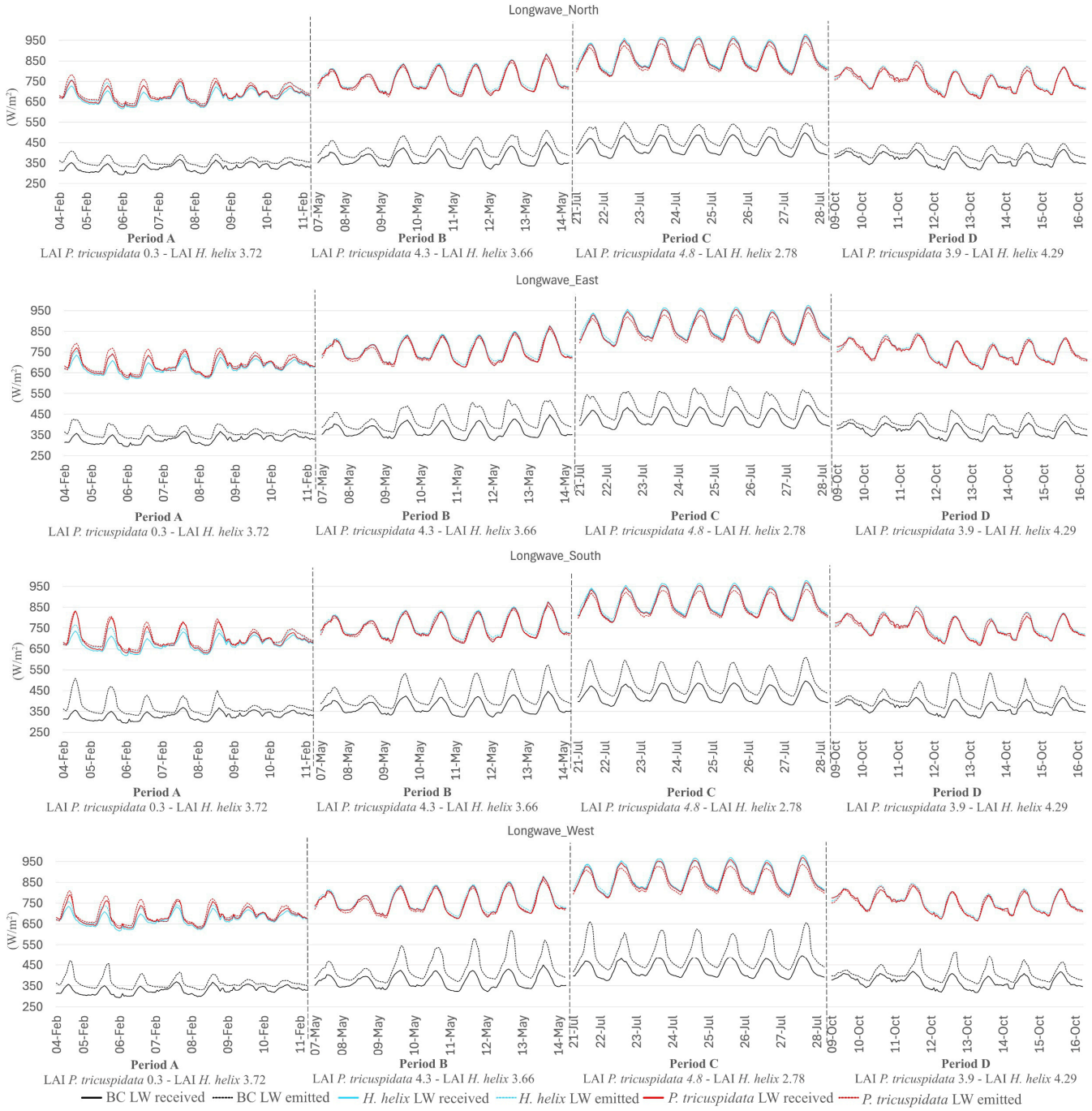


Figure 11. Longwave radiation received and emitted for the four wall orientations, with reference to four different periods.

During Period B, longwave radiation increased relative to Period A for all orientations. On the bare wall, received radiation ranged from 320 to 453 W m^{-2}, while emitted radiation varied between 363 and 619 W m^{-2} on the south and west façades and 362 and 519 W m^{-2} on the north and east façades. Façades covered with *H. helix* showed higher values, with a received radiation of 677–886 W m^{-2} across all orientations and emitted radiation of 688–878 W m^{-2} on the south and east façades. *P. tricuspidata* followed the same pattern, with slightly lower magnitudes than *H. helix*.

Period C exhibited the highest longwave radiation levels of all periods. For the bare wall, received radiation ranged from 372 to 497 W m^{-2}, while emitted radiation peaked on the west façade (417–661 W m^{-2}). Vegetated façades showed the same spatial pattern but

with markedly larger magnitudes. *H. helix* recorded a received radiation of 780–980 W m^{-2} and emitted radiation of 790–962 W m^{-2}, with maxima on the south and east façades. *P. tricuspidata* presented comparable values, with a received radiation of 776–969 W m^{-2} and emitted radiation of 773–940 W m^{-2}, which was particularly high on the east façade.

In Period D, longwave radiation decreased markedly compared to Periods B and C. On the bare wall, received radiation ranged from 317 to 417 W m^{-2} and emitted radiation from 357 to 535 W m^{-2}. Both vegetated configurations showed similar received radiation (664–832 W m^{-2}); however, *H. helix* exhibited slightly higher emitted radiation than *P. tricuspidata*, with values between 672 and 855 W m^{-2}.

In general, the lower surface temperature of the green vegetated surface could be attributed to the reduction in the emission of longwave radiation and lower air temperature immediately above the green surface. When comparing the wall orientations, west-facing façades were the most advantageous for reducing wall-emitted longwave radiation and south-facing façades were a close second—especially during Periods B and C. This follows directly from the largest wall-surface temperature (T_0) drops being observed on the west (and then south) orientation.

4.3. PET

Figure 12 shows the distribution of MRT values on the four facades, in the four periods. Figure 11 reveals that variations in MRT closely mirror the fluctuations in PET (Figure 13), confirming the strong radiative control exerted by façade greening on outdoor thermal perception. In all four orientations, periods with the highest MRT peaks—particularly Period C, where MRT frequently exceeded the upper range of the daily cycle—corresponded to the largest PET values and, consequently, to the most severe thermal-stress classes. In the same period, the introduction of vegetation caused a marked reduction in MRT, especially on the west and south façades, where dense foliage substantially lowered mean radiant exposure. This MRT attenuation directly underlies the significant PET drops observed in the same orientations, with *P. tricuspidata* providing reductions of up to 8.0 °C, consistent with its higher LAI and stronger shielding effect. Conversely, during Period A, MRT values were globally lower, and only modest differences appeared between the bare and vegetated façades. This explains why PET reductions remained limited (≈1.0 °C or less), even though shading from *H. helix* slightly reduced radiant load.

Overall, MRT behavior in Figure 11 confirms that façade greening primarily mitigates PET through the reduction in radiative heat gain, and the magnitude of PET improvement in each period and orientation is directly proportional to the corresponding decrease in MRT.

Building on these MRT–PET dynamics, the detailed PET profiles presented in Figure 13 further reflect how radiative conditions, seasonal forcing, and façade orientation jointly shape thermal-perception patterns across the four assessed periods.

Although PET is calculated from MRT, air temperature, wind speed, and relative humidity, these variables form a non-linearly coupled heat-balance system, and therefore their individual values have no standalone interpretive meaning. Analyzing them separately would neither strengthen the results nor reflect their integrated physiological effects. Since the purpose of this study was to assess outdoor thermal comfort near green façades—rather than to unpack the internal thermophysiological model—PET alone was used as the appropriate indicator, and its values were analyzed across the four representative weeks and on different orientations. The PET categories shown in Figure 13 follow the standard Matzarakis–Mayer biometeorological scale [72], which distinguishes six thermal-perception classes, Cold, Slightly Cool, Neutral/Comfortable, Warm, Hot, and Very Hot, ranging from distinctly cold conditions to strong or extreme heat stress.

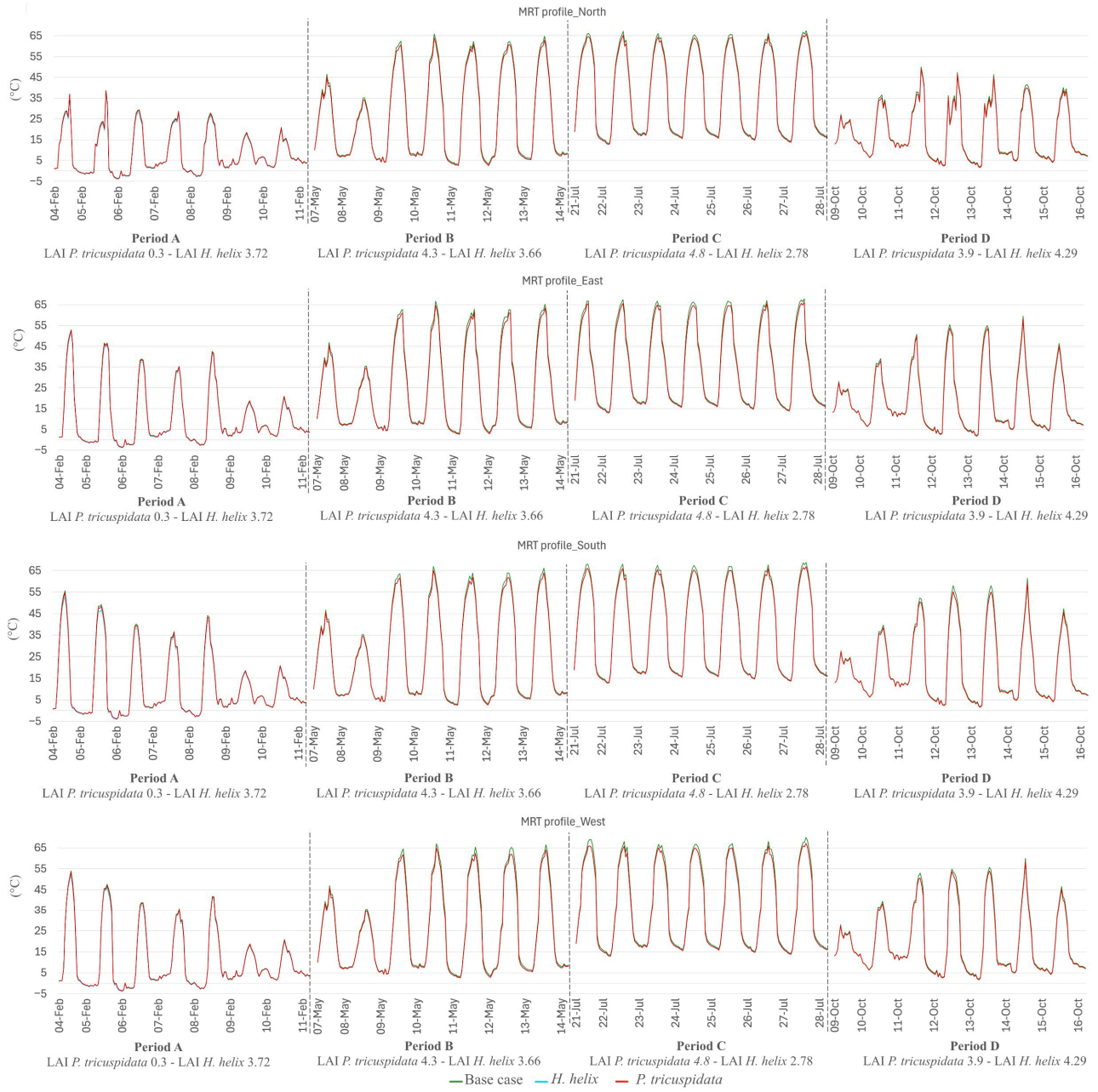


Figure 12. MRT profiles for the four wall orientations, with reference to four different periods.

For the most solar-exposed orientations (south and west), the base case exhibits PET values between 8.0 and 36.0 °C in Period A, dominated by the Cold category. In Period B, PET ranges from 14.0 to 54.0 °C, mainly within the Slightly Cool and Warm classes, while in Period D, values vary from 13.0 to 42.0 °C, again dominated by Slightly Cool and Warm conditions. Period C (July) shows the highest PET values (20.0–58.0 °C), with a prevalence of the Warm and Very Hot categories. The introduction of green façades reduces PET and shifts conditions toward lower thermal classes. In Period C, the *P. tricuspidata* façade produces the largest reductions, reaching up to 3.0 °C on the south exposure and up to 8.0 °C on the west exposure, whereas in Period A *H. helix* yields maximum reductions of approximately 1.0 °C for both orientations.

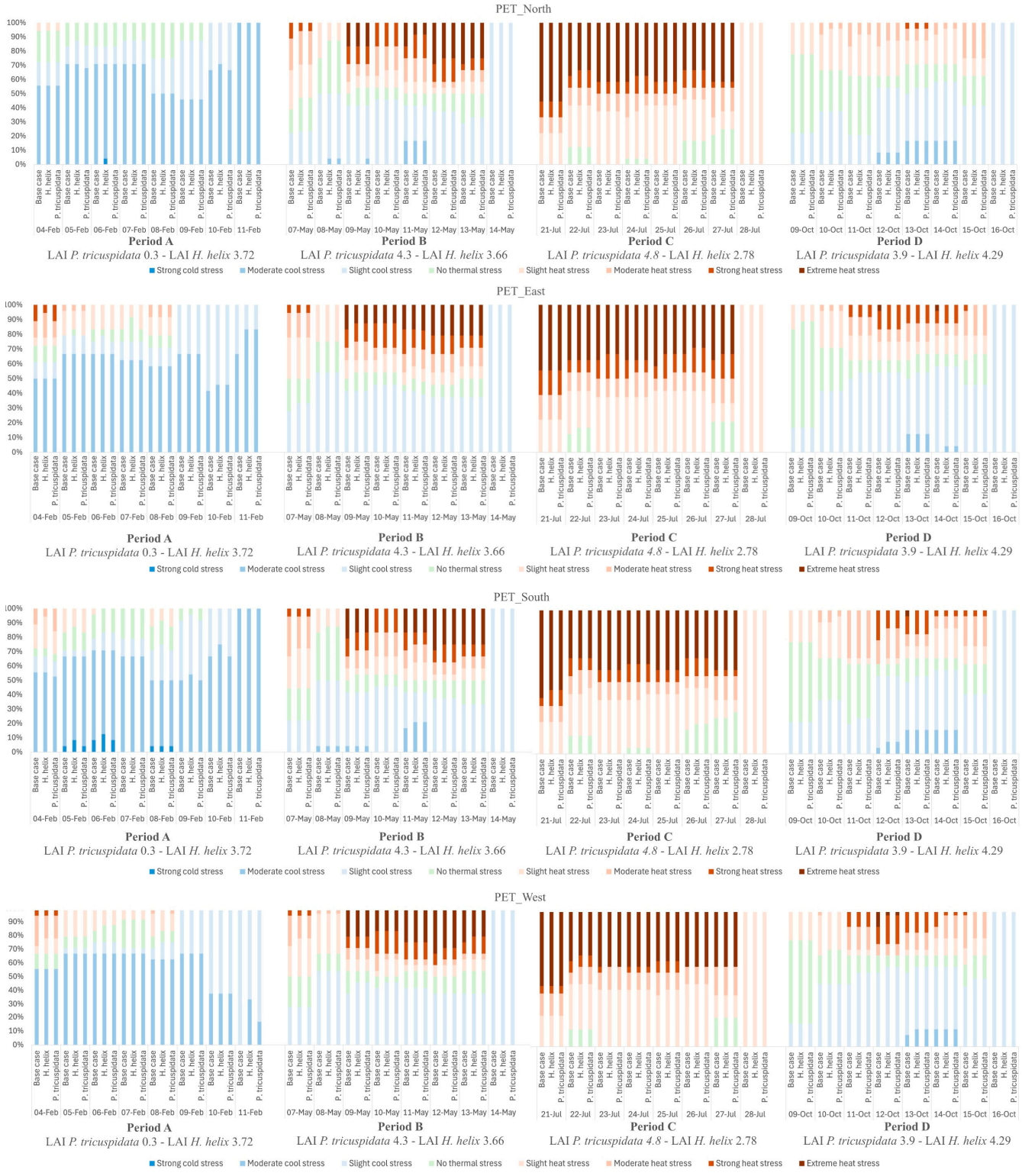


Figure 13. PET profiles for the four wall orientations, with reference to four different periods.

For the north-facing exposure, the base case ranges from 8.0 to 24.0 °C in Period A, with Cold conditions prevailing. In Period B, PET values increase to 16.0–53.0 °C, mainly distributed within the Slightly Cool and Hot/Very Hot categories. During Period C, PET spans 21.0–57.0 °C, dominated by Warm and Very Hot classes, while in Period D, values range from 15.0–38.0 °C, with a prevalence of Slightly Cool and Warm conditions. The east-facing façade shows comparable behavior, with PET values of 9.0–36.0 °C in Period A, 14.0–50.0 °C in Period B, 26.0–58.0 °C in Period C, and 16.0–41.0 °C in Period D,

corresponding to similar dominant thermal classes. Vegetation also reduces PET for the north and east orientations. In Period C, *P. tricuspidata* ensures reductions of up to 4.0 °C, while *H. helix* achieves decreases of up to 3.0 °C on the north façade. In Period A, *H. helix* produces smaller reductions (≈0.3 °C on the north façade and ≈0.9 °C on the east façade). By contrast, *P. tricuspidata* induces a negligible PET increase (<0.1 °C).

According to Table 6, PET variations across the four orientations and time periods are generally modest. During Period A, the north and east façades show negligible PET reductions, with decreases of less than 1.0 °C. The largest PET reduction is observed in Period C (July) on the east-facing façade, with a peak decrease of 6.0 °C on 24 July. For *Hedera helix*, this maximum reduction occurs over short intervals (09:00–11:00, 2 h; and 16:00–17:00, 1 h). *Parthenocissus tricuspidata* shows a comparable response, achieving a slightly greater peak reduction of 6.9 °C on the same date and within the same time windows. By contrast, the smallest reductions occur during Period A on the north façade, where both climbers provide minimal attenuation, with PET decreases of 0.5 °C for *H. helix* and 0.2 °C for *P. tricuspidata.*

Table 6. PET for the four wall orientations, with reference to four different periods, in the base case and green façades.

Period	Orientation	Base Case	*Hedera helix*				*Parthenocissus tricuspidata*			
		PET Range from 9 am to 5 pm (°C)	PET Range from 9 am to 5 pm (°C)	Max °T Reduction (°C)	Date with Maximum °T Reduction	Time with °T Reduction > 10 °C (Duration/h)	PET Range from 9 am to 5 pm (°C)	Max °T Reduction (°C)	Date with Maximum °T Reduction	Time with °T Reduction > 10 °C (Duration/h)
A	North	10.0–24.1	9.9–23.7	0.5	8 February	/	9.9–24.0	0.2	8 February	/
	East	10.6–36.7	10.5–36.1	0.8	4 February	/	10.5–36.5	0.3	4 February	/
	South	9.6–31.5	9.5–30.2	1.3	4 February	12:00–15:00 (3)	9.6–31.0	0.5	4 February	/
	West	9.8–36.2	9.7–35.2	1.2	4 February	15:00–16:00 (1)	9.8–35.8	0.5	4 February	/
B	North	20.9–53.5	20.7–51.1	2.4	13 May	11:00–15:00 (4)	20.7–51.0	2.5	13 May	11:00–16:00 (5)
	East	18.4–50.4	18.2–49.4	1.7	12 May	09:00–13:00 (4)	18.2–49.4	1.7	12 May	09:00–13:00 (4)
	South	20.4–52.4	20.2–50.9	1.5	13 May	11:00–15:00 (4)	20.2–50.9	1.5	13 May	11:00–15:00 (4)
	West	18.7–54.2	18.5–50.3	3.9	12 May	13:00–17:00 (4)	18.5–50.3	3.9	12 May	13:00–17:00 (4)
C	North	36.9–57.9	36.5–57.7	2.5	23 July	14:00–17:00 (3)	36.5–57.7	2.7	23 July	14:00–17:00 (3)
	East	39.6–58.1	38.9–57.9	6.0	24 July	09:00–11:00 (2) 16:00–17:00 (1)	38.8–57.9	6.9	24 July	09:00–11:00 (2) 16:00–17:00 (1)
	South	36.7–58.2	36.3–58.1	2.9	23 July	12:00–14:00 (2)	36.1–58.0	2.9	23 July	12:00–14:00 (2)
	West	34.6–58.3	34.2–58.0	4.8	26-Jul	13:00–17:00 (4)	34.2–58.0	4.8	26 July	13:00–17:00 (4)
D	North	17.2–38.2	17.1–37.4	0.8	13 October	/	17.1–37.4	0.8	13 October	/
	East	20.2–41.3	20.1–40.5	1.4	12 October	09:00–10:00 (1)	20.1–0.5	1.5	12 October	09:00–10:00 (1)
	South	17.1–41.2	17.01–39.6	1.6		11:00–16:00 (5)	17.0–39.6	1.6	13 October	11:00–16:00 (5)
	West	19.3–42.0	19.0–41.3	1.6	12 October	09:00–17:00 (8)	19.0–41.3	1.7	12 October	09:00–17:00 (8)

4.4. Correlation Between Air Temperature, T_0, and PET

Pearson's coefficients (Table 7) show significant, positive correlations ($p < 0.01$) among air temperature (T_{air}), T_0, and PET across all orientations and periods, evidencing coherent thermal forcing: as T_{air} increases, both T_0 and PET rise.

The strength of this response is greatest on the bare wall and attenuated on vegetated façades, with the degree of attenuation modulated by the period-specific leaf area index (LAI).

Correlation values are systematically highest for the bare-wall condition, demonstrating a more direct and unfiltered thermal response to atmospheric warming. In contrast, vegetated façades show weaker—although still strong—correlations, reflecting the capacity of foliage to partially buffer and modulate the transmission of thermal loads. The degree of attenuation is strongly influenced by the LAI: during periods with high LAI (Periods B and C), correlations for *H. helix* and *P. tricuspidata* diverge more distinctly from the bare-wall condition, indicating enhanced shading and evapotranspiration; during low-LAI phases (Period A), correlations converge toward those of the bare wall.

Table 7. Pearson correlation coefficients for T_0 and PET in the base case and green façade configurations, across four orientations and four distinct time periods.

	Period A			Period B			Period C			Period D	
		Air T (°C)			Air T (°C)			Air T (°C)			Air T (°C)
North											
T_0	Base case	0.896 ***	T_0	Base case	0.841 ***	T_0	Base case	0.902 ***	T_0	Base case	0.823 ***
	H. helix	0.721 ***		*H. helix*	0.734 ***		*H. helix*	0.862 ***		*H. helix*	0.621 ***
	P. tricuspidata	0.873 ***		*P. tricuspidata*	0.722 ***		*P. tricuspidata*	0.842 ***		*P. tricuspidata*	0.630 ***
PET	Base case	0.871 ***	PET	Base case	0.890 ***	PET	Base case	0.907 ***	PET	Base case	0.814 ***
	H. helix	0.871 ***		*H. helix*	0.890 ***		*H. helix*	0.907 ***		*H. helix*	0.813 ***
	P. tricuspidata	0.871 ***		*P. tricuspidata*	0.890 ***		*P. tricuspidata*	0.907 ***		*P. tricuspidata*	0.813 ***
East											
T_0	Base case	0.953 ***	T_0	Base case	0.906 ***	T_0	Base case	0.928 ***	T_0	Base case	0.829 ***
	H. helix	0.728 ***		*H. helix*	0.733 ***		*H. helix*	0.870 ***		*H. helix*	0.617 ***
	P. tricuspidata	0.929 ***		*P. tricuspidata*	0.719 ***		*P. tricuspidata*	0.835 ***		*P. tricuspidata.*	0.627 ***
PET	Base case	0.924 ***	PET	Base case	0.906 ***	PET	Base case	0.901 ***	PET	Base case	0.819 ***
	H. helix	0.924 ***		*H. helix*	0.905 ***		*H. helix*	0.898 ***		*H. helix*	0.822 ***
	P. tricuspidata	0.924 ***		*P. tricuspidata*	0.905 ***		*P. tricuspidata*	0.898 ***		*P. tricuspidata*	0.822 ***
South											
T_0	Base case	0.900 ***	T_0	Base case	0.877 ***	T_0	Base case	0.909 ***	T_0	Base case	0.776 ***
	H. helix	0.743 ***		*H. helix*	0.726 ***		*H. helix*	0.857 ***		*H. helix*	0.633 ***
	P. tricuspidata.	0.881 ***		*P. tricuspidata*	0.713 ***		*P. tricuspidata.*	0.832 ***		*P. tricuspidata.*	0.645 ***
PET	Base case	0.931 ***	PET	Base case	0.893 ***	PET	Base case	0.915 ***	PET	Base case	0.809 ***
	H. helix	0.932 ***		*H. helix*	0.892 ***		*H. helix*	0.912 ***		*H. helix*	0.813 ***
	P. tricuspidata	0.931 ***		*P. tricuspidata*	0.892 ***		*P. tricuspidata*	0.912 ***		*P. tricuspidata*	0.813 ***
West											
T_0	Base case	0.769 ***	T_0	Base case	0.798 ***	T_0	Base case	0.785 ***	T_0	Base case	0.707 ***
	H. helix	0.726 ***		*H. helix*	0.730 ***		*H. helix*	0.846 ***		*H. helix*	0.619 ***
	P. tricuspidata	0.786 ***		*P. tricuspidata*	0.719 ***		*P. tricuspidata*	0.827 ***		*P. tricuspidata*	0.627 ***
PET	Base case	0.912 ***	PET	Base case	0.913 ***	PET	Base case	0.920 ***	PET	Base case	0.806 ***
	H. helix	0.915 ***		*H. helix*	0.913 ***		*H. helix*	0.919 ***		*H. helix*	0.810 ***
	P. tricuspidata	0.913 ***		*P. tricuspidata*	0.913 ***		*P. tricuspidata*	0.919 ***		*P. tricuspidata*	0.810 ***

*** Correlation is highly statistically significant at the 0.001 level.

During Period A (Figure 14), correlations are positive and statistically significant but weaker than in warmer periods, reflecting reduced solar forcing. Coupling between air temperature (T_a) and bare-wall T_0 is stronger than that between T_a and vegetated T_0, indicating partial thermal attenuation by green façades even under low forcing. For *Parthenocissus tricuspidata*, this attenuation remains limited in Period A. On the south façade, PET shows the strongest correlation (Figure 15).

In Period B, correlations increase relative to Period A due to enhanced solar radiation. The east façade exhibits the highest base-case correlations, whereas the west façade remains the lowest, despite a relative increase. On the west façade, PET shows the strongest correlation among configurations, while *Hedera helix* correlations are weaker than in Period A. Period C represents the maximum correlation phase between T_a and both T_0 and PET. The east façade shows very strong coupling in the base case, with elevated correlations also observed for *H. helix* and *P. tricuspidata*. Although still the weakest, correlations on the west façade exceed those of Periods A and B; PET correlations on the west façade are the strongest, surpassing Period B values.

In Period D, correlations slightly decrease. Strong base-case correlations persist on the east façade, whereas vegetated configurations (*H. helix* and *P. tricuspidata*) show their highest correlations on the south façade. PET correlations also decline relative to other periods, with maximum values remaining on the east façade.

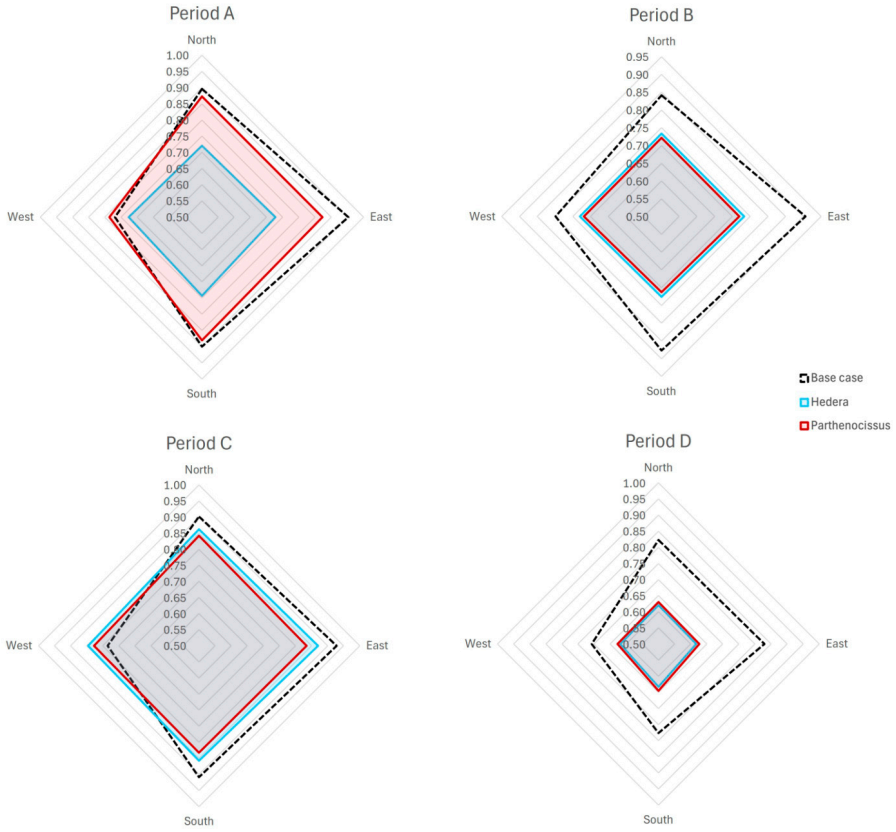


Figure 14. Comparative analysis of Pearson correlation coefficient profiles for T_0 parameters across four wall orientations, with reference to four distinct time periods.

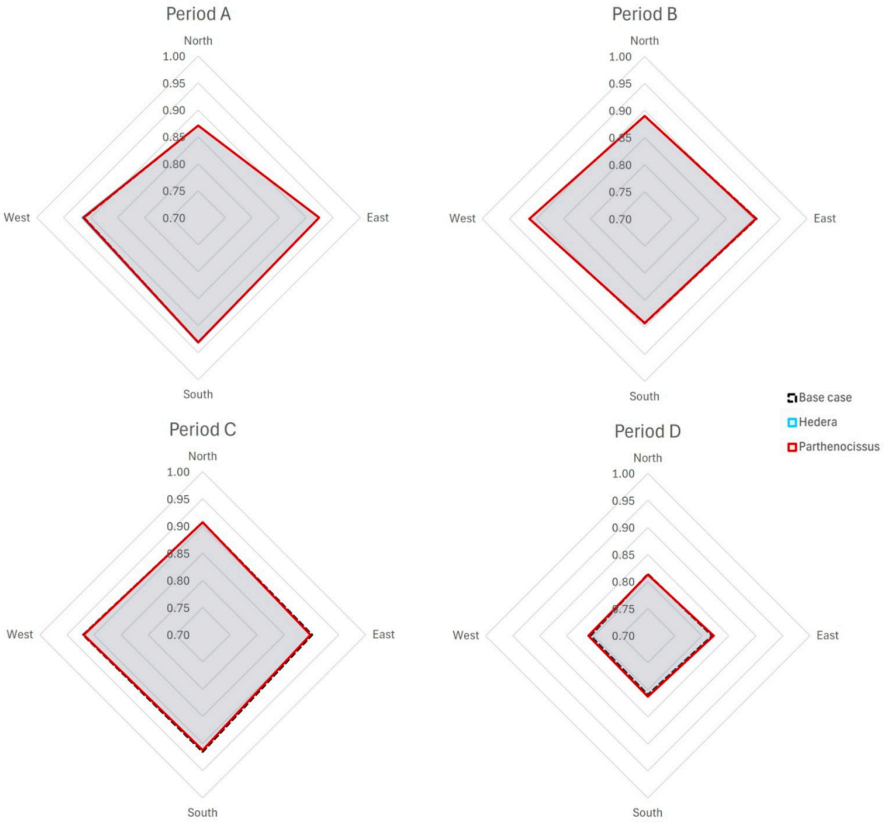


Figure 15. Comparative analysis of Pearson correlation coefficient profiles for PET parameters across four wall orientations, with reference to four distinct time periods.

5. Discussion

Based on the results, several key observations can be drawn.

Period A shows a pronounced divergence in T_0 trends, mainly driven by differences in leaf area index (LAI) between the two climbers. *Parthenocissus tricuspidata* underwent a leafless phase lasting approximately January–March, during which LAI theoretically approached zero but, in practice, ranged between 0 and 1. In this study, LAI was set to 0.30 to account for perennial branches and residual winter foliage, explaining the reduced yet persistent thermal effect. During Period A (mean air temperature 9.1 °C; relative humidity 89.9%), T_0 profiles of the bare wall and *P. tricuspidata* were similar, whereas in all other periods, the two climbers behaved comparably. At peak conditions, the maximum temperature difference between the vegetated façades reached 16.5 °C, reflecting the limited shading capacity of *P. tricuspidata* in winter. The resulting increase in solar gains may have favored passive heating, while façades covered with *Hedera helix* maintained lower T_0 and reduced longwave radiation exchange, likely due to evapotranspiration. Although this provides physical protection, it limits passive solar gains during winter.

During Period B, both species activated and rapidly developed foliage, particularly *P. tricuspidata*, whose LAI increased from 0.30 to 4.30. In the selected May week (mean temperature 17.3 °C; relative humidity 73.3%), the bare wall exhibited elevated T_0, especially on the north and east façades, with two daytime peaks between 12:00 and 14:00. In contrast, façades covered with *H. helix* and *P. tricuspidata* showed similar, more uniform thermal profiles due to high LAI values (3.66 and 4.30), which enhance shading and evapotranspirative cooling. Consequently, daytime heating was attenuated, and the diurnal thermal amplitude was reduced to ~10.0 °C across all orientations, unlike the pronounced fluctuations observed on the bare wall.

During Period C (mean temperature 26.4 °C; relative humidity 70.2%), LAI variations closely tracked increased air temperature and solar radiation. *P. tricuspidata* reached full development (LAI = 4.80), ensuring complete wall coverage and achieving substantial reductions in T_0. *H. helix* was less effective because of its lower LAI, with an average T_0 difference of ~2.0 °C between species across all orientations, confirming the superior summer performance of *P. tricuspidata.*

During Period D (mean air temperature 16.3 °C; relative humidity 84.8%), T_0 decreased overall and exhibited a more heterogeneous temporal pattern. *H. helix* and *P. tricuspidata* displayed nearly identical thermal behavior—the only period in which their performance converged—owing to their comparable LAI values (4.29 and 3.90). Differences were mainly related to foliage albedo (0.20 for *H. helix*; 0.18 for *P. tricuspidata*). Compared to earlier periods, nighttime cooling of the wall beneath vegetation was slower, indicating reduced radiative losses and heat retention by the green façade, which delayed surface cooling. The solar-shading effect can thus be interpreted as the reduction in incident solar radiation reaching the wall surface due to the presence of the green façade, and as the resulting decrease in wall-surface temperature, which is the aspect directly represented in T_0 and longwave radiation graphs (Figures 10 and 11).

According to the results, the cooling mechanisms associated with green façades operate through two partially independent processes: radiative shading, which reduces direct shortwave gains on the wall surface, and evapotranspiration, which contributes to cooling the canopy air layer through latent heat flux. In periods and orientations with intense solar forcing (particularly south and west façades in Periods B and C), radiative shading is the dominant process, as evidenced by the largest reductions in T_0 values, coinciding with peak incoming shortwave radiation.

By contrast, evapotranspiration contributed more consistently to air-temperature moderation, especially under high-LAI conditions and during warm, humid summer

weeks (namely period C), where the cooling of the canopy air layer persisted beyond peak irradiance hours.

This mechanism explains why PET decreases did not always match the timing or magnitude of T_0 reductions: T_0 attenuation was primarily radiative, whereas PET improvements also depended on evapotranspiration-driven reductions in local air temperature and mean radiant temperature. The combined interpretation underscores that peak daytime cooling is led mainly by shading, while extended thermal comfort benefits in the canopy layer are linked to evapotranspiration, particularly evident in *P. tricuspidata* coverage.

Our results demonstrate that when façades are fully vegetated across all orientations and LAI values are high, the resulting temperature reductions fall at the upper end of the ranges reported in empirical field studies (Eumorfopoulou & Kontoleon 2009 [32]; Jim 2015 [59]). In this context, the present study not only confirms these findings but also quantitatively extends the known variability by explicitly linking the magnitude of cooling effects to LAI, seasonal plant dynamics, and façade orientation.

Across all orientations and periods, LAI exerts the strongest control on T_0, with ±20–30% seasonal variations in LAI producing changes of approximately ±2–6 °C in daytime wall-surface temperature reductions, depending on orientation and forcing conditions. By contrast, albedo changes modify T_0 only marginally, generally within the order of ±0.3–1.0 °C, even under strong color shifts such as the autumn transition of *P. tricuspidata*. Similarly, PET displays moderate sensitivity to LAI (typically ±0.5–2.0 °C for reasonable LAI deviations), whereas sensitivity to leaf albedo is negligible relative to the radiative and physiological drivers. These considerations confirm that the core conclusions of the study—especially the seasonal contrast between evergreen and deciduous species and the orientation-dependent cooling—remain robust under plausible variations in LAI and albedo.

The analysis further shows that during Periods B, C, and D, east-oriented green façades reached their daily temperature peaks approximately one hour later than the bare wall, owing to combined shading and reduced radiative heat exchange that delayed morning heating. Overall, both species provide clear benefits: *Parthenocissus tricuspidata* is more effective in mitigating summer overheating, whereas *Hedera helix* contributes more during colder periods.

Our findings regarding the role of LAI and the seasonal behavior of the two climbing species—although still not directly comparable with in situ measurements—are consistent with the existing literature on green façades. As previously highlighted in the manuscript, Pérez et al. (2022) [40] report a clear relationship between LAI and wall-surface temperature (T_0) reduction, demonstrating that façades with higher LAI values achieve substantially greater cooling effects. Furthermore, Jim (2015) [59] and Pérez et al. (2017) [42] show that both LAI and façade orientation jointly govern shading performance, in agreement with the orientation-specific patterns observed in our simulations. Building on these insights, the present study reinforces and extends previous knowledge by providing annual-scale, multi-season ENVI-met simulations that demonstrate how LAI-driven effects persist across full climatic variability, highlighting the importance of species phenology in determining façade-scale thermal behavior.

Beyond surface temperature reduction, green façades also improve outdoor thermal comfort. For all orientations, both species enhance comfort conditions for occupants located 1 m from the wall, with PET variations largely controlled by seasonal thermo-hygrometric conditions and species-specific phenology.

During Period A (mean air temperature 9.1 °C; relative humidity 89.9%), *H. helix* reduces PET by ~1.0 °C, mainly through reduced radiative exchange. Conversely, *P. tricuspidata* induces a slight PET increase (<0.1 °C), which may be beneficial under cold and humid conditions by promoting a marginally warmer thermal perception.

In Period B (mean air temperature 17.3 °C; relative humidity 73.3%), both species show comparable LAI values and PET responses. Under these moderate conditions typical of a Cfa climate, green façades reduce PET and enhance outdoor thermal comfort.

In Period C (mean air temperature 26.6 °C; relative humidity 70.1%), high temperature and humidity dominate PET, limiting human evaporative cooling. Under these conditions, *P. tricuspidata* achieves larger PET reductions than *H. helix*, more effectively mitigating perceived heat stress.

In Period D (mean air temperature 16.1 °C; relative humidity 86.1%), both species exhibit similar PET responses. Green façades provide moderate temperature reductions and improve comfort, although the effect is weaker than in warmer periods.

With regard to PET reduction and outdoor thermal comfort, the comparison with existing studies (Lehnert et al. [38]; Dehghan Lotfabad et al. [39]) shows PET decreases fully consistent with our results. This agreement strengthens the evidence that PET mitigation is closely linked to seasonal variations in LAI and to species-specific phenological dynamics—an aspect that remains only marginally addressed in previous research.

6. Limitations

Several limitations should be acknowledged. This study focuses on plants growing directly on walls (green façades) and deliberately excludes the potential thermal contributions of substrate layers in modular living walls. These limitations open opportunities for further investigations aimed at comparatively assessing the thermal contribution of green façades and living wall systems.

The modeling framework presents an additional limitation because, by focusing on a single, isolated building, the study does not capture the complexity of real urban environments where interactions such as canyon effects and multiple reflections significantly alter the energy balance. Therefore, the conclusions are intended to be applied strictly to the building-envelope scale.

Computational constraints limited the simulations to a $1 \times 1 \times 1$ grid resolution and required the use of default wall and roof properties. Future research will address how different building materials and envelope technologies influence the thermal behavior of green façades.

Leaf area index and albedo values, which in this study rely on data from the literature due to the absence of on-site sensor verification, inevitably introduce uncertainties. These parameters exhibit substantial variability related to site-specific climatic conditions, to the age and maturity of the vegetation and to the state of the sky. Consequently, the use of generalized values may limit the accuracy of model outcomes. Future research should therefore incorporate year-round, species-specific calibration to better capture seasonal dynamics and improve the reliability of simulation inputs. In addition, the microclimatic simulations exhibited systematic, temperature-dependent biases, notably an underestimation of evapotranspirative cooling for both green façade configurations, as reported in previous studies.

The use of NASA POWER data also represents a limitation due to its coarse spatial resolution (~50 km × 50 km) and associated uncertainties, particularly in relative humidity. Finally, PET calculations were performed exclusively at the building-envelope scale. This constitutes an important limitation, as the results reflect only the microclimatic influence of the façade and its immediate surroundings, while broader urban-scale factors—such as street-canyon geometry, surrounding buildings, material properties, and other elements of urban morphology—were not considered. Future studies should expand the boundary conditions to more accurately evaluate the influence of green façades on PET within realistic urban contexts. Additional on-site measurements, particularly of wind speed and airflow

patterns during summer conditions, are also needed to strengthen the reliability of PET estimates and to capture ventilation-driven effects that ENVI-met may not fully resolve under simplified boundary conditions.

7. Conclusions

This study demonstrates that green façades serve as an effective passive strategy for mitigating wall-surface temperatures, enhancing outdoor thermal-comfort perception in the immediate vicinity, and modulating both radiative and convective heat exchanges.

Building on the mechanistic insights discussed above, the results confirm that vegetation-induced shading and evapotranspiration jointly contribute to façade-scale cooling, with effects that vary seasonally and by species.

A comprehensive ENVI-met microclimatic simulation—covering 2016 h (168 h per period per three façades' types) hours with an average speed of 0.65 simulated hours per real hour—was conducted across four representative periods to investigate the influence of key plant functional traits, including evergreen versus deciduous habit, LAI variability, leaf coloration, and longwave radiation exchange properties of vertical greenery.

To respond to the specific research questions, different conclusions can be drawn.

In response to Research Questions 1 and 2, both *Hedera helix* and *Parthenocissus tricuspidata* demonstrably and consistently outperformed bare walls in terms of wall-surface temperature (T_0) reduction. Thermal performance was primarily governed by façade orientation and seasonal climatic conditions. *H. helix* delivered the most stable and reliable cooling effect throughout the year due to its evergreen habit and limited LAI variability, emerging as an effective solution for year-round mitigation, including west-facing façades. Conversely, *P. tricuspidata* provided more effective cooling during the warmer season due to its high peak LAI values. However, its performance dropped sharply during dormancy, when the absence of leaves limited its cooling capacity—while simultaneously allowing beneficial heat gains in winter—highlighting the strong seasonal dependence of deciduous climbers.

Addressing Research Question 3, post-sunset analyses confirm that green façades generally do not induce additional nocturnal heat retention under peak summer conditions, while only a limited and transitional delay in surface cooling may occur during intermediate periods. Both species promoted efficient dissipation of daytime heat, with nighttime cooling rates that remained comparable to bare walls in summer, while a modest delay could occur under transitional conditions (Period D). These results demonstrate that vegetated façades mitigate daytime thermal stress without compromising nighttime thermal release under peak summer conditions.

Regarding Research Question 4, the findings clearly establish foliage density as a key driver of longwave radiation exchange. High LAI values significantly enhanced both emitted and received longwave radiation by reducing the sky view factor and increasing the view fraction toward high-emissivity foliage surfaces. This radiative modulation contributed to improved outdoor thermal perception, as reflected by consistent reductions in PET values, through its interaction with surface temperatures and local microclimatic conditions. PET benefits were maximized on east-facing façades during periods of intense solar forcing, with *P. tricuspidata* providing stronger summer reductions and *H. helix* ensuring more uniform comfort improvements across seasons.

Taken together, the results explicitly indicate that green façade performance is maximized through species-specific and orientation-sensitive design strategies. The strategic integration of evergreen and deciduous climbers enables the optimization of seasonal cooling, outdoor comfort, and façade-scale energy balance, reinforcing green façades as a critical component of climate-adaptive and energy-efficient urban design.

Future research should prioritize long-term, in situ model calibration using mature climber specimens, supported by annual monitoring campaigns capable of capturing the full seasonal dynamics of vegetation. Such continuous datasets—particularly those including direct measurements of stomatal conductance, foliage density, and microclimatic interactions—would allow research to more reliably couple numerical simulations with empirical evidence. By integrating ENVI-met outputs with high-resolution, real-world measurements collected over complete annual cycles, predictive reliability can be substantially improved. This approach would also enable a more accurate evaluation of how climbing species, façade materials, envelope technologies, shading strategies, and other passive design solutions shape the thermal performance of green façades, thereby strengthening their optimized application within climate-responsive building design.

Future research should progressively incorporate these findings into more complex, high-density urban morphologies in order to more accurately assess façade performance within real-world metropolitan environments.

Author Contributions: Conceptualization, B.G., L.R. and A.P.; methodology, B.G.; software, L.R.; validation, BG., L.R. and S.M.; formal analysis, B.G. and L.R.; investigation, B.G., L.R. and S.M.; resources, B.G., L.R., S.M. and A.P.; data curation, L.R. and S.M.; writing—original draft preparation, B.G. and L.R.; writing—review and editing, L.R., S.M. and A.P.; visualization, L.R. and S.M.; supervision, B.G. All authors have read and agreed to the published version of the manuscript.

Funding: This research received no external funding.

Institutional Review Board Statement: Not applicable.

Informed Consent Statement: Not applicable.

Data Availability Statement: Reported results are available upon request.

Acknowledgments: During the preparation of this manuscript, the authors used Copilot Version V5.9.0 for text proofreading purposes. The authors have reviewed and edited the output and take full responsibility for the content of this publication.

Conflicts of Interest: The authors declare no conflicts of interest.

References

1. Cuce, P.M.; Cuce, E.; Santamouris, M. Towards sustainable and climate-resilient cities: Mitigating urban heat islands through green infrastructure. *Sustainability* **2025**, *17*, 1303. [CrossRef]
2. Berardi, U.; GhaffarianHoseini, A.; Ghaffarian Hoseini, A. State-of-the-art analysis of the environmental benefits of green roofs. *Appl. Energy* **2014**, *115*, 411–428. [CrossRef]
3. De Cristo, E.; Evangelisti, L.; Barbaro, L.; De Lieto Vollaro, R.; Asdrubali, F. A Systematic Review of Green Roofs' Thermal and Energy Performance in the Mediterranean Region. *Energies* **2025**, *18*, 2517. [CrossRef]
4. Lai, D.; Liu, W.; Gan, T.; Liu, K.; Chen, Q. A review of mitigating strategies to improve the thermal environment and thermal comfort in urban outdoor spaces. *Sci. Total Environ.* **2019**, *661*, 337–353. [CrossRef]
5. Cui, Y.; Tang, J.; He, B.J. Progressive trend, conceptual terminology, and future directions of green façade research: A review of literature in 2010–2023. *Int. J. Environ. Sci. Technol.* **2025**, *22*, 10991–11010. [CrossRef]
6. Janhäll, S. Review on urban vegetation and particle air pollution—Deposition and dispersion. *Atmos. Environ.* **2015**, *105*, 130–137. [CrossRef]
7. Cai, B.; Cheng, H.; Xiang, F.; Wang, H.; Kang, T. Modeling the Effects of Vegetation on Air Purification Through Computational Fluid Dynamics in Different Neighborhoods of Beijing. *Buildings* **2025**, *15*, 995. [CrossRef]
8. Medl, A.; Stangl, R.; Florineth, F. Vertical greening systems—A review on recent technologies and research advancement. *Build. Environ.* **2017**, *125*, 227–239. [CrossRef]
9. Coma, J.; Perez, G.; de Gracia, A.; Burés, S.; Urrestarazu, M.; Cabeza, L.F. Vertical greenery systems for energy savings in buildings: A comparative study between green walls and green façades. *Build. Environ.* **2017**, *111*, 228–237. [CrossRef]

10. Song, X.; Hao, X.; Lin, Y.; Ai, G.; Yin, W.; Hu, J.; Zhang, S. Energy performance assessment on vertical greening systems with green roof in hot summer and cold winter regions based on long-term experimental data. *Urban For. Urban Green.* **2025**, *103*, 128597. [CrossRef]
11. Radić, M.; Brković Dodig, M.; Auer, T. Green façades and living walls—A review establishing the classification of construction types and mapping the benefits. *Sustainability* **2019**, *11*, 4579. [CrossRef]
12. Perini, K.; Ottelé, M.; Haas, E.; Raiteri, R. Greening the building envelope, façade greening and living wall systems. *Open J. Ecol.* **2011**, *1*, 1–8. [CrossRef]
13. Masi, F. Green walls and green roof—Some experiences from the field. In *Emerging Developments in Constructed Wetlands*; Kumar Yadav, A., Vymazal, J., Zhao, Y., Srivastava, P., Eds.; Elsevier: Amsterdam, The Netherlands, 2025; pp. 447–461.
14. Manso, M.; Castro-Gomes, J. Green wall systems: A review of their characteristics. *Renew. Sustain. Energy Rev.* **2015**, *41*, 863–871. [CrossRef]
15. Pérez, G.; Rincón, L.; Vila, A.; González, J.M.; Cabeza, L.F. Behaviour of green façades in Mediterranean Continental climate. *Energy Convers. Manag.* **2011**, *52*, 1861–1867. [CrossRef]
16. Djedjig, R.; Belarbi, R.; Bozonnet, E. Experimental study of green walls impacts on buildings in summer and winter under an oceanic climate. *Energy Build.* **2017**, *150*, 403–411. [CrossRef]
17. Bianco, L.; Serra, V.; Larcher, F.; Perino, M. Thermal behaviour assessment of a novel vertical greenery module system: First results of a long-term monitoring campaign in an outdoor test cell. *Energy Effic.* **2017**, *10*, 625–638. [CrossRef]
18. Kumar, P.; Debele, S.E.; Khalili, S.; Halios, C.H.; Sahani, J.; Aghamohammadi, N.; Andrade, M.F.; Athanassiadou, M.; Bhui, K.; Calvillo, N.; et al. Urban heat mitigation by green and blue infrastructure: Drivers, effectiveness, and future needs. *Innovation* **2024**, *5*, 100588. [CrossRef]
19. Teh, C.; Henson, I.E.; Goh, K.; Husni, M. The effect of leaf shape on the interception of solar radiation. *J. Plant Physiol.* **2006**, *1*, 12–27.
20. Pianella, A.; Aye, L.; Chen, Z.; Williams, N.S.G. Substrate Depth, Vegetation and Irrigation Affect Green Roof Thermal Performance in a Mediterranean Type Climate. *Sustainability* **2017**, *9*, 1451. [CrossRef]
21. Xu, H.; Chen, H.; Qian, C.; Li, J. The Evapotranspiration Characteristics and Evaporative Cooling Effects of Different Vegetation Types on an Intensive Green Roof: Dynamic Performance Under Different Weather Conditions. *Sustainability* **2024**, *16*, 10812. [CrossRef]
22. Ascione, F.; De Masi, R.F.; Mastellone, M.; Ruggiero, S.; Vanoli, G.P. Green Walls, a Critical Review: Knowledge Gaps, Design Parameters, Thermal Performances and Multi-Criteria Design Approaches. *Energies* **2020**, *13*, 2296. [CrossRef]
23. Bakhshoodeh, R.; Ocampo, C.; Oldham, C. Exploring the evapotranspirative cooling effect of a green façade. *Sustain. Cities Soc.* **2022**, *81*, 103822. [CrossRef]
24. Li, H.; Zhao, Y.; Sützl, B.; Kubilay, A.; Carmeliet, J. Impact of green walls on ventilation and heat removal from street canyons: Coupling of thermal and aerodynamic resistance. *Build. Environ.* **2022**, *214*, 108945. [CrossRef]
25. Ottelé, K.; Perini, E.; Haas, M. Life cycle assessment (LCA) of green façades and living wall systems. In *Eco-Efficient Construction and Building Materials*; Pacheco-Torgal, F., Cabeza, L.F., Labrincha, J., de Magalhães, A., Eds.; Woodhead Publishing: Cambridge, UK, 2014; pp. 457–483.
26. Shafiee, E.; Faizi, M.; Yazdanfar, S.; Khanmohammadi, M.A. Assessment of the effect of living wall systems on the improvement of the urban heat island phenomenon. *Build. Environ.* **2020**, *181*, 106923. [CrossRef]
27. Victorero, F.; Vera, S.; Bustamante, W.; Tori, F.; Bonilla, C.; Gironás, J.; Rojas, V. Experimental study of the thermal performance of living walls under semiarid climatic conditions. *Energy Procedia* **2015**, *78*, 3416–3421. [CrossRef]
28. Salah, G.M.J.A.; Romanova, A. Life cycle assessment of felt system living green wall: Cradle to grave case study. *Environ. Chall.* **2021**, *3*, 100046. [CrossRef]
29. Bustami, R.; Belusko, M.; Ward, J.; Beecham, S. Vertical greenery systems: A systematic review of research trends. *Build. Environ.* **2018**, *146*, 226–237. [CrossRef]
30. Lin, H.; Li, X. The Role of Urban Green Spaces in Mitigating the Urban Heat Island Effect: A Systematic Review from the Perspective of Types and Mechanisms. *Sustainability* **2025**, *17*, 6132. [CrossRef]
31. Manso, M.; Teotónio, I.; Silva, C.M.; Cruz, C.O. Green roof and green wall benefits and costs: A review of the quantitative evidence. *Renew. Sustain. Energy Rev.* **2021**, *135*, 110111. [CrossRef]
32. Eumorfopoulou, E.A.; Kontoleon, K.J. Experimental approach to the contribution of plant-covered walls to the thermal behaviour of building envelopes. *Build. Environ.* **2009**, *44*, 1024–1038. [CrossRef]
33. Priya, U.K.; Senthil, R. Passive cooling of residential buildings in tropical climates using user-preferred plant species in green walls. *J. Build. Eng.* **2025**, *107*, 112732. [CrossRef]
34. He, Y.; Ren, C.; Mak, H.; Lin, C.; Wang, Z.; Fung, J.; Li, Y.; Lau, A.; Ng, E. Investigations of high-density urban boundary layer under summer prevailing wind conditions with Doppler LiDAR: A case study in Hong Kong. *Urban Clim.* **2021**, *38*, 100884. [CrossRef]

35. Carlo, O.C.; Fellini, S.; Palusci, O.; Marro, M.; Salizzoni, P.; Buccolieri, R. Influence of obstacles on urban canyon ventilation and air pollutant concentration: An experimental assessment. *Build. Environ.* **2024**, *250*, 111143. [CrossRef]
36. Jiang, G.; Wu, M.; Li, H.; Wu, Y. Mechanism of Wind and Buoyancy Driving on Ventilation and Pollutant Transport in an Idealized Urban Street Canyon. *Buildings* **2024**, *14*, 3168. [CrossRef]
37. Baş, H.; Andrianne, T.; Reiter, S. City configurations to optimise pedestrian level ventilation and wind comfort. *Sustain. Cities Soc.* **2024**, *114*, 105745. [CrossRef]
38. Lehnert, M.; Kremser, J.; Janků, Z.; Květoňová, V.; Geletič, J. Assessing green walls' effects on outdoor human thermal exposure in temperate climate cities. *Sci. Rep.* **2025**, *15*, 42053. [CrossRef]
39. Dehghan Lotfabad, A.; Hosseini, S.M.; Dabove, P.; Heiranipour, M.; Sommese, F. Impacts of Vertical Greenery on Outdoor Thermal Comfort and Carbon Emission Reduction at the Urban Scale in Turin, Italy. *Buildings* **2025**, *15*, 450. [CrossRef]
40. Pérez, G.; Coma, J.; Chàfer, M.; Cabeza, F.F. Seasonal influence of leaf area index (LAI) other energy performance of a green façade. *Build. Environ.* **2022**, *207*, 108497. [CrossRef]
41. Poiss, M.; Briefer, A.; Scharf, B.; Spörl, P.; Stangl, R. Vertical greenery as natural shading of glass façades: Bioshading coefficients for 4 climbing plant species for assessment of shading performance. *Build. Environ.* **2025**, *283*, 113399. [CrossRef]
42. Pérez, G.; Coma, J.; Sol, S.; Cabeza, L.F. Green façade for energy savings in buildings: The influence of leaf area index and façade orientation on the shadow effect. *Appl. Energy* **2017**, *187*, 424–437. [CrossRef]
43. Ghasaban, M.; Mirjalili, P.; Yeganeh, M. Integration of building envelope with open spaces and greenery to enhance thermal and visual comfort and energy efficiency in office buildings. *Results Eng.* **2025**, *25*, 103660. [CrossRef]
44. Poddar, D.; Park, S.; Chang, S. Energy performance analysis of a dormitory building based on different orientations and seasonal variations of leaf area index. *Energy Effic.* **2017**, *10*, 887–903. [CrossRef]
45. Ansari, A.Q.; Loomis, W.E. Leaf Temperatures. *Am. J. Bot.* **1959**, *6*, 713–717. [CrossRef]
46. Moss, R.A.; Loomis, W.E. Absorption Spectra of Leaves. I. The Visible Spectrum. *Plant Physiol.* **1952**, *27*, 370–391. [CrossRef] [PubMed]
47. Gates, D.M. Leaf temperature and energy exchange. *Arch. Meteorol. Geophys. Bioklimatol. Ser. B* **1962**, *12*, 321–336. [CrossRef]
48. Cuimin, L.; Wei, J.; Li, C. Influence of foliage thickness on thermal performance of green façades in hot and humid climate. *Energy Build.* **2019**, *199*, 72–87. [CrossRef]
49. Heinrichs, S.; Schmidt, W. Dynamics of *Hedera helix* L. in Central European beech forests on limestone: Results from long-term monitoring and experimental studies. *Plant Ecol.* **2015**, *216*, 1–15. [CrossRef]
50. Pichlhöfer, A.; Korjenic, A.; Sulejmanovski, A.; Streit, E. Influence of Façade Greening with Ivy on Thermal Performance of Masonry Walls. *Sustainability* **2023**, *15*, 9546. [CrossRef]
51. Setiawan, G.D.; Przybysz, A.; Treesubsuntorn, C.; Popek, R. Effect of simulated rain and rain frequency on particulate matter re-accumulation in roadside climbers *Parthenocissus quinquefolia*. *Environ. Pollut.* **2025**, *382*, 126649. [CrossRef]
52. Qi, S.; Utaberta, N.; Kiet, A.L.K.; Yanfang, X.; Xiyao, H. Effects of green façade retrofitting on thermal performance and energy efficiency of existing buildings in northern China: An experimental study. *Energy Build.* **2025**, *335*, 115550. [CrossRef]
53. Di Bacco, M.; Scorzini, A.R. Recent changes in temperature extremes across the north-eastern region of Italy and their relationship with large-scale circulation. *Clim. Res.* **2020**, *81*, 167–185. [CrossRef]
54. Chandler, W.S.; Stackhouse, P.W., Jr.; Hoell, J.M.; Westberg, D.; Zhang, T. NASA prediction of worldwide energy resource high resolution meteorology data for sustainable building design. In Proceedings of the Solar 2013 Conference of American Solar Energy Society, Baltimore, MD, USA, 16–20 April 2013.
55. Rodrigues, G.C.; Braga, R.P. Evaluation of NASA POWER Reanalysis Products to Estimate Daily Weather Variables in a Hot Summer Mediterranean Climate. *Agronomy* **2021**, *11*, 1207. [CrossRef]
56. Aboelkhair, H.; Mostafa, M.; El Afandi, G. Assessment of agroclimatology NASA POWER reanalysis datasets for temperature types and relative humidity at 2 m against ground observations over Egypt. *Adv. Space Res.* **2019**, *64*, 129–142. [CrossRef]
57. Monteiro, A.L.; Sentelhas, P.C.; Pedra, G.U. Assessment of NASA/POWER satellite-based weather system for Brazilian conditions and its impact on sugarcane yield simulation. *Int. J. Climatol.* **2018**, *38*, 1571–1581. [CrossRef]
58. Qin, H.; Zhou, B. Optimizing Vegetation Configurations for Seasonal Thermal Comfort in Campus Courtyards: An ENVI-Met Study in Hot Summer and Cold Winter Climates. *Plants* **2025**, *14*, 1670. [CrossRef] [PubMed]
59. Jim, C.Y. Thermal performance of climber greenwalls: Effects of solar irradiance and orientation. *Appl. Energy* **2015**, *154*, 631–643. [CrossRef]
60. Fang, H.; Baret, F.; Plummer, S.; Schaepman-Strub, G. An overview of global leaf area index (LAI): Methods, products, validation, and applications. *Rev. Geophys.* **2019**, *57*, 739–799. [CrossRef]
61. Campiotti, C.A.; Giagnacovo, G.; Latini, A.; Mariani, S.; Sperandei, M.; Pace, S.; Campiotti, A.; Di Bonito, R.; Marone, A. *Gli ecosistemi Vegetali per la Rigenerazione Ecologica Delle Città*; Rapporto Tecnico ENEA-RT-2021-13; ENEA: Roma, Italy, 2021.
62. He, Y.; Lin, E.S.; Yu, Z.; Tan, C.L.; Yok Tan, P.; Hien Wong, N. The effect of dynamic albedos of plant canopy on thermal performance of rooftop greenery: A case study in Singapore. *Build. Environ.* **2021**, *205*, 108247. [CrossRef]

63. Chen, C. Determining the Leaf Emissivity of Three Crops by Infrared Thermometry. *Sensors* **2015**, *15*, 11387–11401. [CrossRef]
64. Liu, Z.; Zheng, S.; Zhao, L. Evaluation of the ENVI-Met Vegetation Model of Four Common Tree Species in a Subtropical Hot-Humid Area. *Atmosphere* **2018**, *9*, 198. [CrossRef]
65. Deardorff, J.W. Efficient prediction of ground surface temperature and moisture with inclusion of a layer of vegetation. *J. Geophys. Res.* **1978**, *83*, 1889–1903. [CrossRef]
66. Jacobs, C.M.J. Direct Impact of Atmospheric CO_2 Enrichment on Regional Transpiration. Ph.D. Thesis, Wageningen Agricultural University, Wageningen, The Netherlands, 1994.
67. Ciacci, C.; Banti, N.; Di Naso, V.; Bazzocchi, F. Evaluating UHI Mitigation and Outdoor Comfort in a Heritage Context: A Microclimate Simulation Study of Florence's Historic Center. *Sustainability* **2025**, *17*, 8760. [CrossRef]
68. Liu, T.; Wang, Y.; Zhang, L.; Xu, N.; Tang, F. Outdoor Thermal Comfort Research and Its Implications for Landscape Architecture: A Systematic Review. *Sustainability* **2025**, *17*, 2330. [CrossRef]
69. Staiger, H.; Laschewski, G.; Matzarakis, A. Selection of Appropriate Thermal Indices for Applications in Human Biometeorological Studies. *Atmosphere* **2019**, *10*, 18. [CrossRef]
70. Bröde, P.; Fiala, D.; Błazejczyk, K.; Holmér, I.; Jendritzky, G.; Kampmann, B.; Tinz, B.; Havenith, G. Deriving the Operational Procedure for the Universal Thermal Climate Index (UTCI). *Int. J. Biometeorol.* **2012**, *56*, 481–494. [CrossRef] [PubMed]
71. Blazejczyk, K.; Epstein, Y.; Jendritzky, G.; Staiger, H.; Tinz, B. Comparison of UTCI to Selected Thermal Indices. *Int. J. Biometeorol.* **2012**, *56*, 515–535. [CrossRef] [PubMed]
72. Matzarakis, A.; Mayer, H.; Iziomon, M.G. Applications of a universal thermal index: Physiological equivalent temperature. *Int. J. Biometeorol.* **1999**, *43*, 76–84. [CrossRef]
73. Mendes, P.T.; Nouri, A.S.; Matzarakis, A. Evaluating Outdoor Human Thermal Comfort Through Climate-Resilient Adaptation: A Case Study at School of Science and Technology (NOVA FCT) Campus. *Atmosphere* **2025**, *16*, 677. [CrossRef]
74. Qiao, L. Study on the Dynamic Heat Transfer Role of Vertical Greening in Building Microclimate Based on Multi-Objective Coupling. *J. Renew. Sustain. Energy* **2025**, *17*, 025101. [CrossRef]
75. Bruse, M.; Fleer, H. Simulating Surface–Plant–Air Interactions inside Urban Environments with a Three Dimensional Numerical Model. *Environ. Model. Softw.* **1998**, *13*, 373–384. [CrossRef]
76. Simon, H.; Lindén, J.; Hoffmann, D.; Braun, P.; Bruse, M.; Esper, J. Modeling transpiration and leaf temperature of urban trees—A case study evaluating the microclimate model ENVI-met against measurement data. *Landsc. Urban Plann.* **2018**, *174*, 33–40. [CrossRef]
77. Bruse, M.; Helge, S.; Sinsel, T. Development and Implementation of a High-Resolution Dynamical Wall and Roof Model for ENVI-met. Part 2: Vegetated Walls and Roofs. 18 September 2023. Available online: https://doi.org/10.13140/RG.2.2.36020.83842 (accessed on 14 January 2026).

Disclaimer/Publisher's Note: The statements, opinions and data contained in all publications are solely those of the individual author(s) and contributor(s) and not of MDPI and/or the editor(s). MDPI and/or the editor(s) disclaim responsibility for any injury to people or property resulting from any ideas, methods, instructions or products referred to in the content.